Centre for Geo-Information

Thesis Report GIRS-2005-15

MAPPING HYDROCARBON SEEPAGES IN THE NIGER DELTA USING ASTER PRODUCTS.

FRANK UDO EKPENYONG

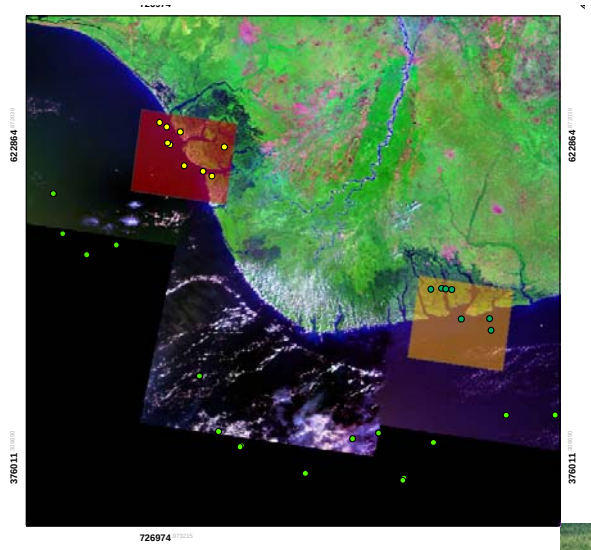

May 2005

WAGENINGEN UNIVERSITY
WAGENINGEN UR

MAPPING HYDROCARBON SEEPAGES IN THE NIGER DELTA

USING ASTER PRODUCTS

FRANK UDO EKPENYONG

MAY, 2005

SIGNATURE (SUPERVISOR)

……

SIGNATURE (PROGRAM COORDINATOR)

……

SIGNATURE (STUDENT)

……

MAPPING HYDROCARBON SEEPAGES IN THE NIGER DELTA

USING ASTER PRODUCTS

FRANK UDO EKPENYONG

Registration number: 800108219040

Supervisor:

PROF. DR. MICHAEL SCHAEPMAN

A thesis submitted in partial fulfillment for the award of the degree of Master of Science (Geo-Information Science) at The Centre for Geo-Information, Wageningen University and Research Centre, The Netherlands.

May, 2005
Wageningen, The Netherlands

Thesis code number: GRS-80337
Wageningen University and Research Centre
Laboratory of Geo-Information Science and Remote Sensing
Thesis Report: GIRS-2005-15

Acknowledgement

My utmost gratitude goes to God Almighty, for being my unceasing source of inspiration and knowledge; and for making the impossible a reality. I herein express my indebtedness to TOTALFINAELF Petroleum Unlimited, Port Harcourt for granting me this unrivalled opportunity (financial assistance) to undertake postgraduate studies. Next acknowledgement is made to Prof. Dr. Michael Schaepman (my supervisor) for his invaluable suggestions, criticisms, cooperation, support and patience during my research work and whose wide scope of knowledge and experience I have been able to tap from. I am deeply indebted to Ing. Willy ten Haaf (Study Advisor) for his love, advice, encouragement and support in every form. I am also thankful to Dr. Jan Clevers and Weimar Acerbi for their services as members of board of examiners for my Thesis. Many thanks to all the staff members of the Centre for Geo-Information for their support throughout my studies in one way or the other they have contributed to my success.

I always be grateful to my parents, Mr. Udo Ekpenyong and Mrs. Elizabeth Ekpenyong , they laid the right foundation for what I have achieved today; I am so thankful to Uchenna Aduaka, she is really a friend to count on all times.

Profound gratitude also goes to Elder Eton and Pastor Elder Udim Inyang; their prayers have been so helpful. Lastly I also grateful to all individuals whose moral, spiritual, psycho-emotional and material support helped in no small way to make this work possible.

DEDICATION

This work is dedicated to my parents –

Mr Udo Samuel Ekpenyong and Mrs Elizabeth Ekpenyong

ABSTRACT

Hydrocarbon seepages occurrences are well known all over the world and historical references to hydrocarbon seepages date back to earliest recorded history. Historically, natural hydrocarbon seeps have provided a useful tool for petroleum exploration. Hydrocarbon seepages occurrence provides surface or sub-surface expressions that makes it possible to detect using different direct or indirect exploration methods. The surface expressions can take many forms, including microbiological anomalies and the formation of "paraffin dirt"; mineralogic changes such as formation of calcite, pyrite, uranium, elemental sulfur, and certain magnetic iron oxides and sulfides; bleaching of red beds; clay mineral alteration; electrochemical changes; radiation anomalies; and biogeo-chemical and geobotanical anomalies.

Satellite-based remote sensing of hydrocarbon-induced alterations is one of the exploration methods being use to map areas of hydrocarbon seepage occurrences all over the world. The method provides a synoptic view needed to study the spatial variability that occurs in areas of seepage occurrences and holds great promise as a rapid, cost-effective means of remote detection of anomalous diagenesis in surface soils and rocks.

Hydrocarbon-induced alterations are one of the major causes of surface spatial variability in the study area-oil rich Niger delta part of Nigeria. The surface expressions of hydrocarbon seeps is best developed in areas with numerous well-devolved migration pathways and an active petroleum system like that present in the Niger Delta.

The study demonstrates the potentials of The Advanced Spaceborne Thermal Emission and Reflection (ASTER) products in mapping hydrocarbon seepage detection. The Visible Near-Infrared (VNIR) and Shortwave Infrared (SWIR) on-demand products (images) of ASTER were used in the study. Three approaches were adopted in the study; onshore hydrocarbon seepage mapping, offshore

hydrocarbon seepage mapping and the columnar hydrocarbon seepage mapping.

For the onshore hydrocarbon seepage mapping approach, image unmixing and Principal Component Analysis (PCA) methods were employed. A normalized hydrocarbon index was developed and used in the offshore hydrocarbon mapping approach while the SAM target detection and equalisation with k-means classification was employed in mapping columnar associated hydrocarbon seepages.

Carbonates minerals - calcite and dolomite were identified to be the dominant type of mineral constituent onshore. This is could be associated to the active hydrocarbon system of the study areas; however other reasons could also be responsible. The band ratio proved to be effective in mapping variability over the water body this could be due to the almost homogenous nature of the water body. Mapped variability offshore needs to be validated before concluding that it indicates the presence of hydrocarbon or source of variability is the hydrocarbon related activities or occurrences onshore. The columnar mapping approach maps those pixels associated with the hydrocarbon flares noticed on the test sites, the wind speed and direction was integrated to allocate map columnar hydrocarbon cloud to hydrocarbon flares.

TABLE OF CONTENT

LIST OF FIGURES

LIST OF TABLES

ABBREVIATIONS

AL-OH	Aluminium Hydroxide
ASTER	Advanced Spaceborne Thermal Emission and Reflection
AST07	Level 2 Surface Reflectance data set
AVIRIS	Airborne Visible and Infrared Imaging Spectrometer
BBOE	Billion Barrels of Oil Equivalent
ENVI	Environmental for the Visualisation of images
EOS	Earth Observing System
HC	Hydrocarbon
HYMAP	Hyperspectral Mapper
NASA	National Aeronautics and Space Administration
NDVI	Normalized Difference Vegetation Index
PC	Principal Component
PCA	Principal Component Analysis
REE	Rare-Earth Elements
SAM	Spectral Angle Mapper
SWIR	Shortwave Infrared
TM	Thematic Mapper (Landsat)
TIR	Thermal Infrared
USGS	United States Geological Survey
VNIR	Visible Near Infrared

CHAPTER ONE

1.0 INTRODUCTION

The Occurrence of Natural hydrocarbon seeps are a well known all over the world and historical references to seepage date back to earliest recorded history. Asphalt from seeps in the Middle East has been used as a building material since 3,000 BC, and burning gas seeps in the Baku region were known from several centuries before Christ [Hunt, 1979]. Documented written records of seeps include biblical references, and the works of Herodotus and Marco Polo [Wilson *et al*., 1974]. Historically, natural hydrocarbon seeps have provided a useful tool for petroleum exploration [Link, 1952; Hunt, 1979; Tedesco, 1995].

Link [1952] states that the significance of seeps from an exploration standpoint is that they prove the presence of source hydrocarbons and suitable structural traps for their accumulation. The presence of hydrocarbon seeps at the Earth surface indicates that hydrocarbon reservoirs leaks, leakage can be active or passive, visible to the human eye (macroseepage) or only chemically detected (microseepage), [van der Werff and Arko Lucieer, 2003]. The presence of hydrocarbon is necessary for hydrocarbon seepage, and this requires a sufficient thickness of sedimentary rock and source rocks for hydrocarbon generation within the sedimentary section. The leakage of hydrocarbon and associated fluids to the surface is responsible for a number of chemical alterations in rocks and soils that overlay oil and gas reservoirs (Almeida-Filho et al., 1999 and Almieda-Filho, 2002).

Due to the presence of different pressures in the Earth subsurface, hydrocarbons can migrate from deep surface reservoirs to shallower levels and eventually to the surface. It is important to note that the migration of heavier hydrocarbons needs more space; possible paths are reservoirs rocks acting as carrier bed, unconformities, tectonic structure that breach reservoirs or seals, and surface expressions of intrusions such as mud volcanoes and salt domes

[link, 1952]. Long term leakage can lead to formation of anomalous oxidation-reduction zones [van der Werff and Arko Lucieer, 2003]. The reducing environment created by microseepage phenomenon can convert limonitic minerals to the ferrous state, resulting in bleaching of red beds, feldspar can be converted to clay minerals (kaolinite, illite, chlorite) (Almeida-Filho et al., 1999). Other mineralogical changes can take place in such an environment, such as the formation of calcite, pyrite, uranium, and certain magnetic iron oxides and sulphides (Donovan 1974, Matthews 1986, Segal and Merin 1989, Schumacher 1996). Some of these microseepage-induced minerals exhibit diagnostic spectral features that allow their remote identification (Almeida-Filho et al., 1999). However, the chemical processes involved in seepages and the resulting surface expressions are still not fully understood. Most alterations are not unique for the redox environment of seeping hydrocarbons, which makes them difficult to separate from alterations caused by other soil processes [Schumacher and Abrams, 1996]. Hydrocarbon seeps and its surface expressions are commonly found throughout the world in sedimentary basins containing oil reserves.

The Niger Delta region of Nigeria has a basinal setting which favours the occurrence of various hydrocarbon seepages in the region. This basinal setting includes; the presence of prolific source rock capable of charging large traps; ongoing oil generation and migration, or its occurrence in the geologically-recent past, and the presence of vertical conduits such as salt diapers or faults that reach the surface (Brownfield et al., 1999).

Imaging spectrometry proves to be a good tool for detecting hydrocarbon microseepages. Hyperspectral imagery can successful be used to directly mapping hydrocarbon that are present at the surface [Horig et al., 2001] since heavy hydrocarbons have clear absorption features in the reflective part of the spectrum [Clutis, 1989].

This field of remote sensing measures quantitatively the components of the earth system from calibrated spectra acquired as images for scientific

researches and applications including the detection of hydrocarbon seepages (M. de Jong, and van der Meer 2002)

1.1 PROBLEM DEFINITION

Large quantities of oil and gas from leaking reservoirs reach the surface forming seeps. When visible by the human eye there are called macroseeps, else they are called microseeps. Seeps are relevant to the oil and gas industry as a potential source of information for exploration. Hydrocarbon microseeps give rise to expressions at the earth surface in form of: (1) detectable trace concentrations of gases (mainly Ethane and Methane), (2) mineral alterations of soils and (3) anomalous spectral response in vegetation. (M. de Jong, and van der Meer 2002).

Furthermore surface expressions of hydrocarbon-induced alteration of soils and sediments can take many more forms including (1) microbiological anomalies and the formation of "paraffin dirt"; (2) mineralogic changes such as formation of calcite, pyrite, uranium, elemental sulphur, and certain magnetic iron oxides and sulfides; (3) bleaching of red beds; (4) clay mineral alteration; (5) electrochemical changes; (6) radiation anomalies; and (7) biogeo-chemical and geobotanical anomalies (Schumacher D., 1996).

Detection of hydrocarbon-induced surface manifestations in the form of seepages can be mapped with the aid of remote sensing data gotten from aerial photography, radar, and Landsat Multispectral Scanner (MSS) (Schumacher D., 1996; Donovan T. et al, 1979; Schumacher D., 1999; Van de Meer et al. 2002). With the availability of special imagers dedicated to imaging spectrometry, the mapping of geological units or outcrops becomes easier. Multispectral instruments, such as Landsat, have demonstrated that they can detect subtle geochemical anomalies associated with hydrocarbon seeps. However, these geochemical anomalies are non-specific and could vary, thus some form of validation or field verification is required. In contrast, hyperspectral instruments such as Airborne Visible and Infrared Imaging Spectrometer (AVIRIS) can readily differentiate between ancient hydrocarbon

seeps and active hydrocarbon seeps. High costs, small area of coverage, and need for advanced image processing limit the use of hyperspectral data. The Advanced Spaceborne Thermal Emission and Reflection (ASTER) instrument is an excellent compromise between the two approaches (Staskowski, J., 2004). ASTER is a multispectral instrument, but includes more spectral bands in the shortwave infrared region where minerals associated with hydrocarbon seeps have identifiable absorption features. Remote sensing tools could then be used to map changes in the surface in the form of mineral alterations of soils or map traces of gas concentrations or map anomalous vegetation stress response as a result of occurrence of hydrocarbon seeps in the oil-rich Niger (Ejedawe, 1981) Delta part of Nigeria.

It is important to note that geological exploration data could find their greatest utility when integrated with geological, geophysical and remote sensing data, thus leading to better oil prospect evaluation and risk assessment (Schumacher D., 1999).

1.2 RESEARCH OBJECTIVES

The objective of this research is to assess the potential of ASTER products in mapping hydrocarbon seepages.

1.3 RESEARCH QUESTION

The following research questions are derived from the research objectives;

Can ASTER images be able to map hydrocarbon seepages?

Which method or algorithm aids the detection of oil and gas seepages with ASTER images?

Can the spatial extent of hydrocarbon seepages be mapped with Aster Image?

How are continuous columnar and discrete point hydrocarbon features expressed and visualised?

1.4 RESEARCH HYPOTHESIS

Aster images (products) have potentials for hydrocarbon seepage mapping/detection.

1.5 RESOURCES

Two ASTER level 2A on-demand images namely AST07 is used for the study. The 3 Visible Near Infrared (VNIR) bands and 6 Shortwave Infrared (SWIR) bands that make up AST07 product (image) would be used. The two ASTER Images defined the test sites in the study. Test site I image is described with upper left corner coordinates of 5'48'46'N, 4'52'29'E; upper right corner 5'43'00'N, 5'32'32'E; lower left corner 5'14'56'N, 4'47'40'E; lower right corner 5'09'11'N, 5'10'04'E. Scene cloud coverage for test site I image is 0% and covers western part of Warri state, Nigeria. Test site II image is described with upper left corner coordinates of upper left corner 4'39'14'N, 6'48'24'E; upper right corner 4'33'27'N, 7'28'22'E; lower left corner 4'05'24'N, 6'43'33'E; lower right corner 3'59'37'N,7'23'30'E. Scene cloud coverage is about 2% and covers southern part of Port Harcourt, Rivers state, Nigeria. Both test site I and II were chosen for study because both sites have similar feature (hydrocarbon) and are thus representative of the oil-rich Niger Delta (Ejedawe, 1981). The features found on both sites includes oil terminals, oil-tank farms, hydrocarbon pipeline corridors, know and unknown hydrocarbon occurrence locations, hydrocarbon flares and a combination of land (onshore) and water (offshore) bodies. Some of these features are visible on the test site images while others are not.

The Environmental for the Visualisation of images (ENVI) software was used extensively in the study. ArcGIS software (Arcmap) would be used in visualisation and presentation of the results. Other internet resources related to the topic was also used during the course of the study.

1.6 THESIS STRUCTURE

In chapter one, the study was introduced and a description of the work overview was also presented, these include the problem definition, research

objectives, research questions, resources and thesis structure. Chapter two consist of the state of the art with respect to the problem field, it also deals with prior work, current and recent trends related to the topic.

The Methods and Materials implemented in the study were discussed in Chapter three. The geology of the study area and the data used in the study was discussed here and careful documentation of the entire methodology and its implementation steps were described in chapter three. In chapter four, the results and discussion was discussed. Here the obtained results from the implementation are explained and discussed.

The final chapter discusses the conclusions and recommendations raised from the study. In the conclusion, the results are discussed with regards to the research issues raised in chapter 1.

CHAPTER TWO

2.0 STATE OF THE ART

Remote sensing provides the synoptic views needed to study spatial variability that occurs at landscape, regional and global scales. The spatial variability cut across all earth application fields. Advances in optical remote sensing provide geoscientists with improved methods for identifying and mapping surface mineralogy (Rowan, 2001). It is assumed that hydrocarbon seepages cause changes in the soil air as well as in the soil mineralogy (Noomen et al. 2003) where it occurs.

The leakage of hydrocarbons and associated fluids to the surface is responsible for a number of chemical alterations in rocks and soils that overlay oil and gas reservoirs (Almeida-Filho, 2002). These alterations are one of the major causes of surface spatial variability in the oil rich Niger delta part of Nigeria. The surface variability could be as a result of hydrocarbon gases (microseeps) that seep to the surface (Noomen et al. 2003) or localised visible oil and gas seeps that seeps to the surface in areas containing large concentrations of light hydrocarbons as well as, if available, high-molecular-weight hydrocarbons (Schumacher, 1999). It is a long established fact that hydrocarbons are generated and/or trapped at depth and leak in varying but detectable quantities to the surface, the close association of surface geochemical anomalies with faults and fractures is well known (Schumacher, 1996). The surface expression of hydrocarbon seeps is best developed in areas with numerous well-developed migration pathways and an active petroleum system like that present in the Niger Delta.

A further assumption is that the anomaly at the surface can be related reliably to a petroleum accumulation at depth (Schumacher, 1996). The success to which this assumption can be proved depends on the geology of the area. It becomes more increasingly difficult as the geology becomes complex (van der

Werff and Arko Lucieer, 2003, Schumacher 1999). With the cutting edge technology provided with remote sensing, there exists a great potential of a successful surface mapping of hydrocarbon induced alteration notice on the surface; which can significantly affect the economics of an exploration or development program of oil exploration in an area. But it is also necessary that the user must be aware of some limitations associated with geochemical exploration methods (Schumacher, 1996; 1999). Some limitations of surface geochemical exploration are related to geology; others are related to the method itself (Schumacher, 1996). Limitations related to geology includes: -

- The geochemical expressions of seepage is complex and varied
- There is generally no simple one-to-one correlation between a surface anomaly and a subsurface accumulation
- False seeps anomalies can be caused by reworked hydrocarbons and/or reworked source rocks.
- Reservoirs that are significantly underpressured or contain heavy oil may not be detected by some surface geochemical methods.
- Successful integration of surface geochemical data with subsurface geology becomes increasingly difficult as the geology becomes more complex.

Limitations related to the method includes: -

- Discovery of hydrocarbon induced anomaly does not guarantee discovery of commercial significant volumes of hydrocarbon
- Image pre-processing/processing or use of improper image analysis techniques cause ambiguity that lead to interpretation failures
- Remote sensing based hydrocarbon mapping cannot replace existing exploration technology' however, they can add value to existing geological and geophysical exploration data.

2.1 MECHANISM OF HYDROCARBON SEEPAGE VERSUS REMOTE SENSING

Seepage is divided into macroseepages and microseepages. Macroseepage refers to a macroefussion of hydrocarbons in large quantities such as the massive outpouring or ejection of fluid in an extrusive volcanic flow, while microseepage implies a less voluminous discharge not visible to the naked eye but which can be sensed using enhanced analytical methods (Luyendyk et al., 2003). Another form of seepages are the active and passive seepages; active seepages refers to areas where subsurface hydrocarbons seep in large concentrations into shallow sediments and soils and into the overlying water column, these type of seeps are usually detected by most sampling techniques (Schumacher, 1999). While the passive seeps refers to those areas where subsurface hydrocarbons are not actively seeping.

The surface geochemical expression of petroleum seepage can take many forms (Schumacher, 1996) : -

- Anomalous hydrocarbon concentrations in sediments, soils, water, and even the atmosphere
- Microbiological anomalies and the formation of paraffin dirt
- Anomalous non-hydrocarbon gases such as helium and radon
- Mineralogical changes such as the formation of calcite, pyrite, uranium, elemental sulphur, and certain magnetic iron oxides and sulfides
- Clay mineral alterations
- Radiation anomalies
- Geothermal and hydrologic anomalies
- Bleaching of red beds
- Goebotanical anomalies
- Altered acoustical, electrical, and magnetic properties of soils and sediments

The figure below (fig.2.1) shows a generalized model of hydrocarbon microseepage and hydrocarbon-induced effects on soils and sediments (Schumacher, 1996; 1999; Saunders et al., 1999). Surface geochemical evidence of seepage occurs when light hydrocarbons seep upward from trap creating a reducing a zone; bacteria degradation sets in and results in pyrite and carbonate precipitation. Geophysical anomalies occurring as a result of light hydrocarbon seeps includes high resistivity anomaly, high polarization anomaly, magnetic anomaly and low resistivity anomaly (fig.2.1).

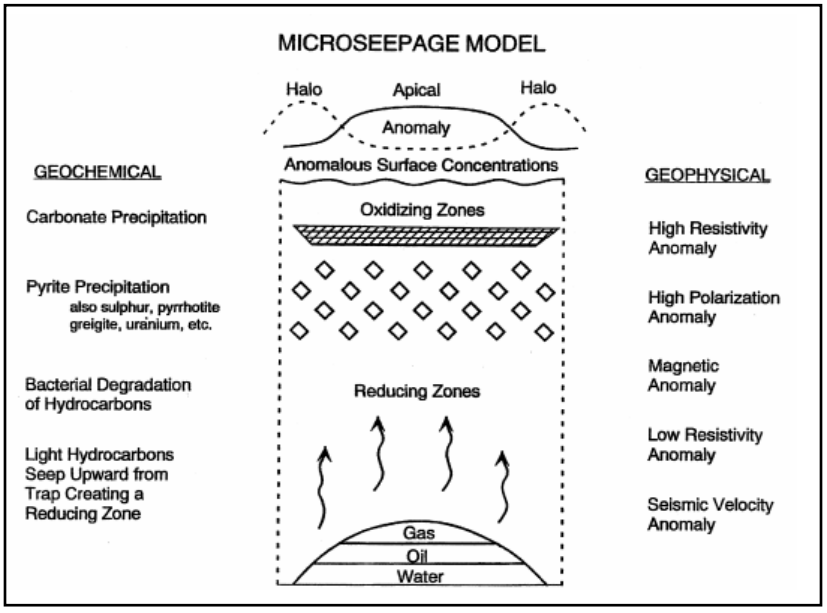

Figure 2.1: Generalized model of hydrocarbon microseepage and hydrocarbon-induced effect soils and sediments (from Schumacher, 1996)

Remote sensing is one of the geochemical exploration techniques been relied upon today in the oil industry. Remote sensing technique focused on the detection of the surface manifestation of hydrocarbon micro or macroseepage can be a complementary prospecting tool, minimizing cost and time in the search for oil and gas reservoirs (Almeida-Filho, 2002). Two gases commonly found in microseeps, methane and carbon dioxide also have clear absorption features in the reflective part of the spectrum (van der Werff and Lucieer, 2003). But the detection of these gases with remote sensing tools are problematic since carbon dioxide is already present in the atmosphere and the absorption features of methane is too narrow to allow detection by present day

airborne instrument, besides hydrocarbon seepages are not the only natural source of methane and carbon dioxide production (van der Werff and Lucieer, 2003). Although direct detection of gases originating from microseeps is problematic, optical remote sensing is an excellent tool for detecting micrseepages-induced alterations (van der Werff and Lucieer, 2003, Schumacher 1999). Most of the surface expressions of hydrocarbon induced seepages are today mapped effectively with remote sensing tools (e.g van der Werff and Arko Lucieer, 2003, Lang et al., 1985, and Crosta et al, 1997). Many of these alterations can be mapped by imaging spectrometers; remote sensing could be a rapid cost-effective means of hydrocarbon exploration when compared to geochemical surveying methods or seismic studies (Van der werff et al., 2003). Almeida-Filho (1999) successfully detected bleached red beds in an approximately 6 km ^{2} area by using band ratios of Landsat TM imagery. According van der Werff and Arko Lucieer, (2003) the results appeared to be consistent with soil gas anomalies (ethane, propane, butane and pentane) that had been measured at the same spot. Satellite-based remote sensing of hydrocarbon-induced alterations holds great promise as a rapid, cost-effective means of detecting anomalous diagenesis in surface soils and rocks (Schumacher, 1996), however on a metre scale, indirect detection is hampered by the same problem as direct detection of seepages; the signal of the subtle and non-unique alterations resulting from hydrocarbons is disturbed by the heterogeneous surface of the earth (van der Werff and Arko Lucieer, 2003). The technical question put forward by van der Werff and Arko Lucieer, (2003) remains – 'how to separate a non-unique, weak signal from a variable background'.

CHAPTER THREE

3.0 MATERIALS AND METHODS

3.0.1 STUDY AREA – PETROLEUM GEOLOGY

The Niger Delta is situated in the Gulf of Guinea (fig. 3.1) and extends throughout the Niger Delta Province as defined by Klett and others (1997). From the Eocene to the present, the delta has prograded southwestward, forming depobelts that represent the most active portion of the delta at each stage of its development (Doust and Omatsola, 1990). These depobelts form one of the largest regressive deltas in the world with an area of some 300,000 km^2 (Kulke, 1995), a sediment volume of 500,000 km^3 (Hospers, 1965), and a sediment thickness of over 10 km in the basin depocenter (Kaplan and others, 1994). The Niger Delta Province contains only one identified petroleum system (Kulke, 1995; Ekweozor and Daukoru, 1994).

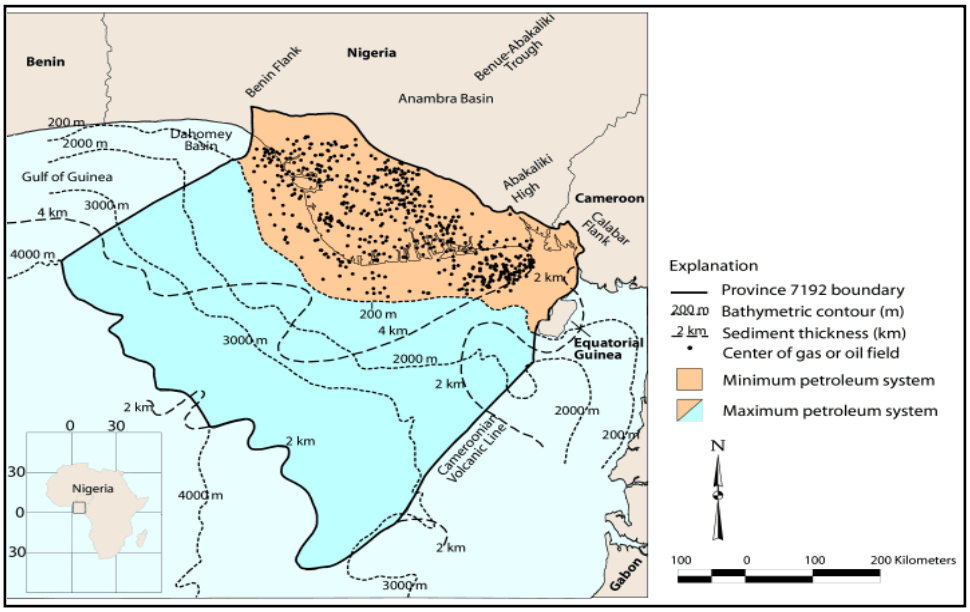

Figure 3.1: showing index map of Nigeria, map of the Niger Delta showing Province outline (maximum petroleum system); bounding structural features; minimum petroleum system as defined by oil and gas field center points (data from petroconsultants, 1996a); 200, 2000, 3000 and 4000m bathymetric contours; 2 and 4km sediment thickness. (source: USGS Open-File Report 99-50_H; Niger delta petroleum system)

This system is referred to as the Tertiary Niger Delta (Akata –Agbada) Petroleum System. The maximum extent of the petroleum system coincides with the boundaries of the Niger Delta province (fig. 3.1). The minimum extent of the system is defined by the aerial extent of fields and contains known resources (cumulative production plus proved reserves) of 34.5 billion barrels of oil (BBO) and 93.8 trillion cubic feet of gas**2** (TCFG) (14.9 billion barrels of oil equivalent, BBOE) (Petroconsultants, 1996). Currently, most of this petroleum is in fields that are onshore or on the continental shelf in waters less than 200 meters deep (fig. 3.1 and fig 3.2), and occurs primarily in large, relatively simple structures. A few giant fields do occur in the delta, the largest contains just over 1.0 BBO (Petroconsultants, Inc., 1996a). Among the provinces ranked in the U.S. Geological Survey's World Energy Assessment (Klett and others, 1997), the Niger Delta province is the twelfth richest in petroleum resources, with 2.2% of the world's discovered oil and 1.4% of the world's discovered gas Petroconsultants, Inc. 1996).

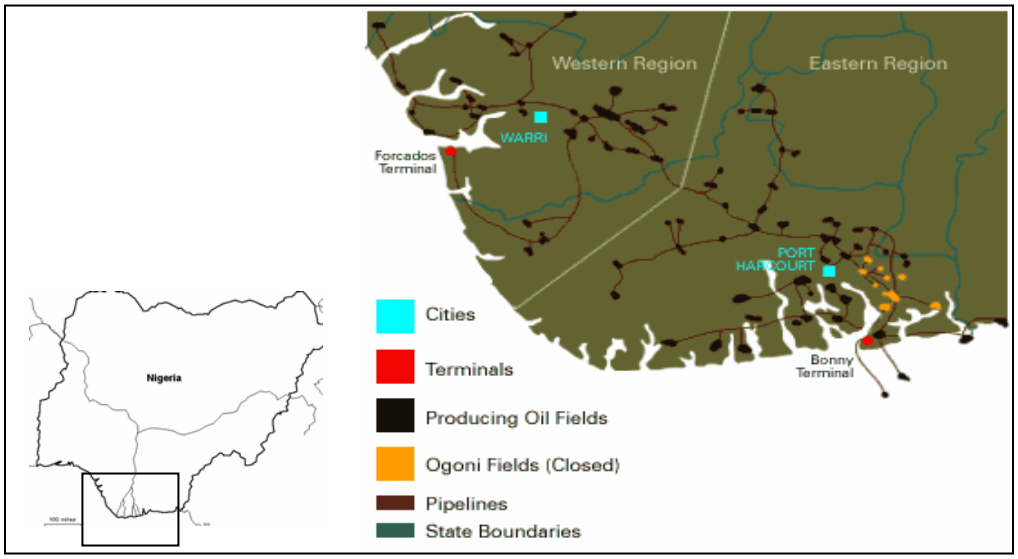

Figure 3.2: showing insert, map of Nigeria and study area showing known oil producing fields, terminals and oil related areas onshore within the Niger Delta (from Ejedawe, 1981)

3.0.2 TEST SITES

Two representative test sites with similar visible features were selected from the Niger Delta for the study. One of the images (fig.3.3) is located on the

western edge of the Niger delta, the Forcados oil Station is situated here. The second image (fig. 3.3) is covers the southern part of the Delta and the Degema/Ogboni oil fields. Both test sites have similar known hydrocarbon features-flares, oil-tank farm (see appendix I for picture of oil-tank), pipeline corridor and were selected because of its excellent exposure of known and unknown oil related activities areas onshore and offshore. Images used in the study were selected using the ASTER browse tool available on the internet called the global visualization Viewer (http://asterweb.jpl.nasa.gov/glovis.asp). With the global viewer two representative cloud free image scenes were selected and ordered through the Earth Observing System (EOS) data gateway available online (http://edcimswww.cr.usgs.gov/pub/imswelcome/).

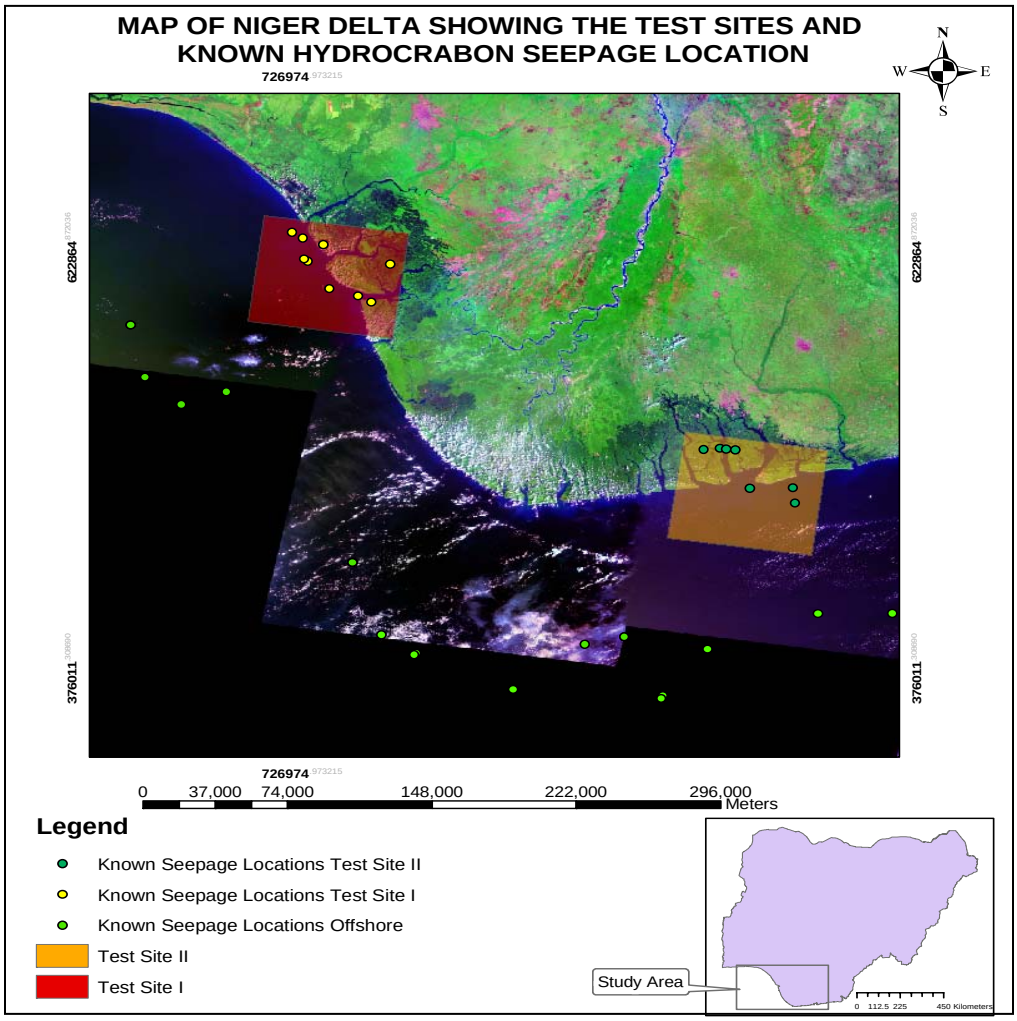

Figure 3.3: Map of Niger Delta showing test sites and known seepage locations within and outside the test sites; insert: map of Nigeria showing study area

3.0.3 DATA

Two ASTER level 2 on-demand surface reflectance data set (AST07) products were used during the study (fig. 3.4 a-d); they contain surface reflectance for Visible Near Infrared (VNIR) and Shortwave Infrared (SWIR) channels at 15-m and 30-m resolutions respectively, derived by applying an atmospheric correction to observed satellite radiances and the data product is recorded as percent reflectance (King et al., 2003).

The ASTER sensor is an imaging instrument currently flying on the Terra satellite (Yamaguchi et al., 1998). It was launched in December 1999 as part of NASA's Earth Observing System (EOS). ASTER contains three separate instrument subsystems (VNIR, SWIR and TIR) with 14 bands from the visible green to the thermal infrared (0.52 – 11.65 μm).

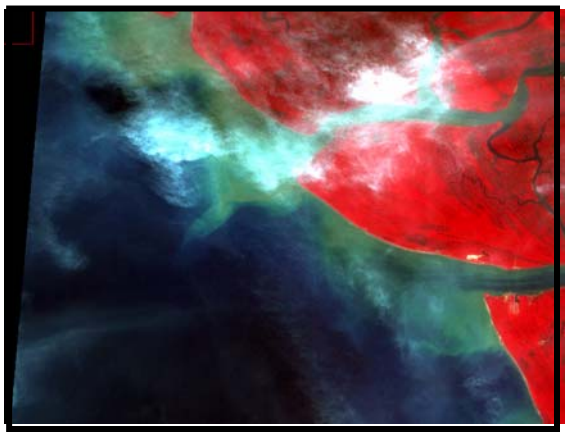

(a) VNIR band: RGB 3N, 2, 1

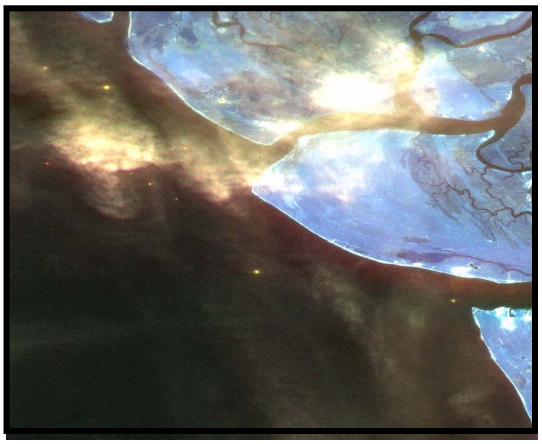

(b) SWIR band: RGB 9, 7, 4

(c) VNIR band: RGB 3N, 2, 1

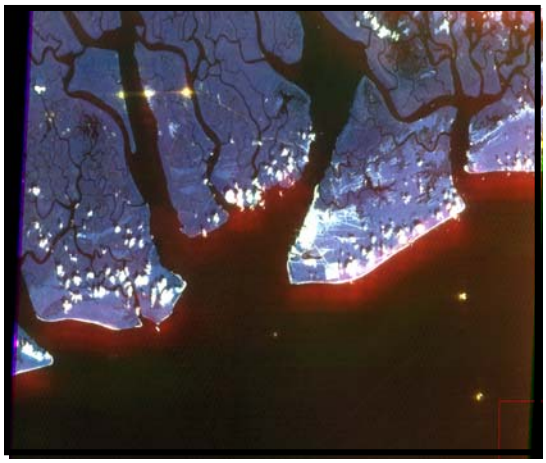

(d) SWIR band: RGB 9, 7, 4

Figure 3.4: (a) test site I, VNIR Image, 15-m resolution (b) test site I, SWIR Image, 30-m resolution (c) test site II, VNIR image, 15-m resolution and (d) test site II, SWIR Image, 30-m resolution

The instrument has a swath width of 60km and a spatial resolution of 15, 30 and 90m/pixel, in the VNIR, SWIR and TIR regions respectively (Kahle et al., 1991). The swath width is 60Km, but ASTER's pointing capability extends the total cross-track viewing capability to 232km (Fujisada, 1995). ASTER measures reflected radiation in three bands between 0.52 and 0.86μm (VNIR) and in six bands from 1.6 to 2.3μm (SWIR). The VNIR, SWIR and TIR wavelengths regions provide complementary data for alteration mapping. The three VNIR bands are important sources of information about absorption in transition metals, especially iron and some rare-earth elements (REE) (Hunt, Salisbury, & Lenhoff, 1972; Rowan, Kingston, & Crowley, 1986), and for chlorophyll absorption in photosynthesising vegetation (Knipling, 1970). In the six SWIR bands carbonate, hydrate and hydroxide mineral spectra display molecular absorption features related to overtones and combination tones (Hunt, 1977). In the SWIR bands minerals associated with hydrocarbon seeps have identifiable absorption features (see table 3.1). ASTER VNIR products would be used mainly for visual aid because of its spatial resolution and sharp contrast between vegetation and other features in both test sites. ASTER SWIR products would be the basis for this study as explained earlier, mineral associated with hydrocarbon seepages show prominent absorption features in the SWIR region. Because other minerals especially iron-bearing and hydrated minerals have distinctive VNIR and SWIR spectra, surface composition mapping is best undertaken with the full range of ASTER bands. ASTER data are inexpensive and effective tool for mapping geochemical anomalies related to hydrocarbon seepage.

Table 3.1: Possible mineral assemblage that can be detected by ASTER SWIR band passes (Scholte et al., 2004).

Absorption wavelength (μm)	Mineral Groups
2.165	Low pH/acid environments
2.205	Al-OH bearing minerals
2.260	Jarosite
2.327	Carbonates and Mg-OH bearing minerals

3.0.4 PREPROCESSING

The ASTER products were all covering the same spatial extent but Visible Near Infrared (VNIR) channel has a spatial resolution of 15m while the Shortwave Infrared (SWIR) channel has a spatial resolution of 30m. The SWIR image was resampled to 15m (same as VNIR) resolution using the nearest neighbourhood method and then combined with the VNIR image. The new image was a combination of the VNIR (3 bands) plus SWIR (6 bands) to have a 9 bands image that is spectrally and spatially rich for the study.

Known mineral associated with all forms of hydrocarbon seepages were selected as endmembers minerals for the study. These endmembers (minerals) were mainly from the carbonate, oxides, inosillicates and sulphate groups, the endmembers were from the ASTER spectral library and resampled to reflect the ASTER spectral response (fig 3.5.)

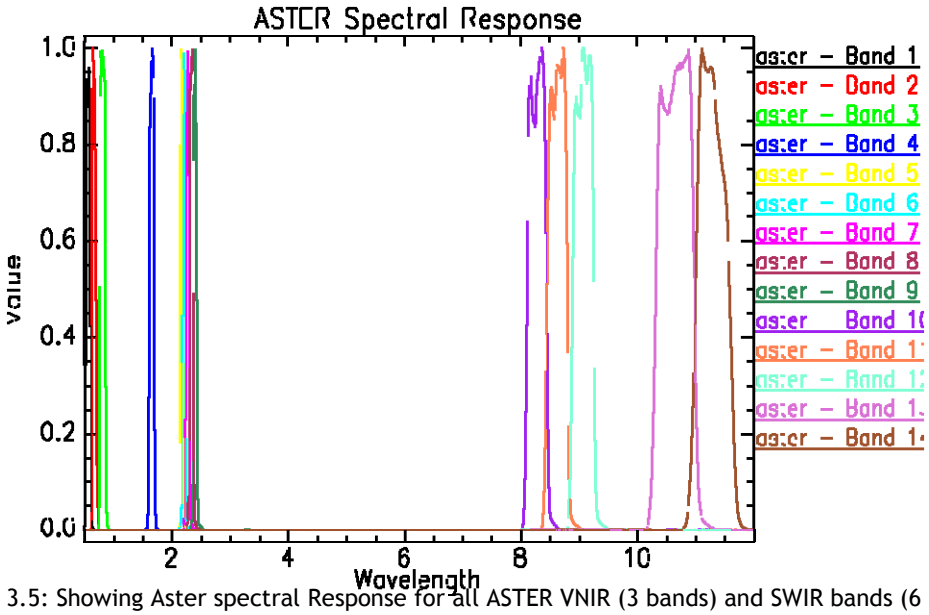

Figure 3.5: Showing Aster spectral Response for all ASTER VNIR (3 bands) and SWIR bands (6 bands)

3.0.5 PROCESSING

Image processing was divided into three approaches; onshore hydrocarbon seepage mapping and quantification; offshore hydrocarbon seepage mapping and quantification and the columnar seepage mapping and quantification (fig 3.6).

The onshore hydrocarbon seepage mapping approach dealt with mapping the textural variations induced as a result of hydrocarbon seepage occurrence. This approach consists of image unmixing and Principal Component Analysis (PCA). The selected endmembers from the ASTER spectral library were resampled to ASTER spectral response and were the input endmembers used during the linear unmixing. The Principal Component Analysis (PCA) was applied to both test sites and the results of the PCA and linear unmixing defined the mapped onshore hydrocarbon seepages; these results were quantified to determine the spatial extent of the mapped seepage.

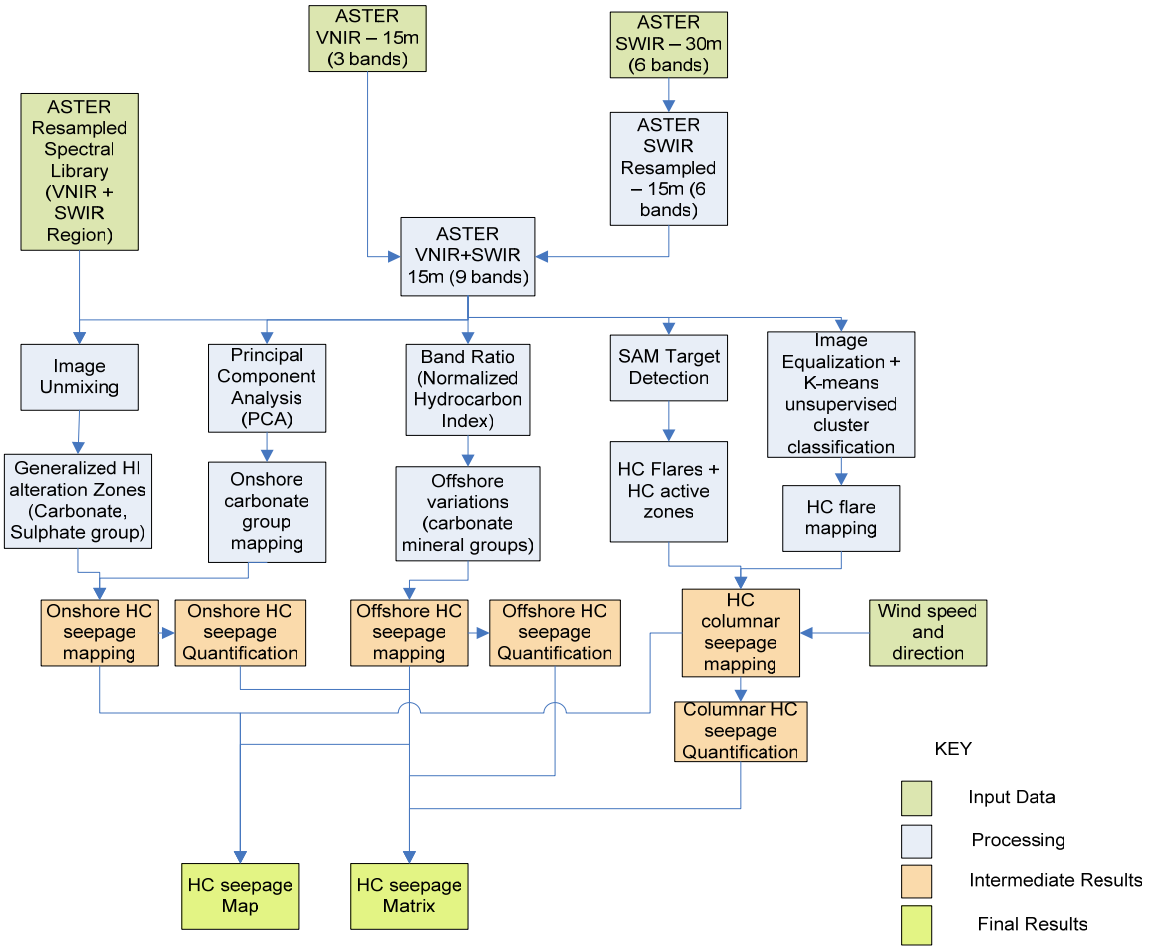

Figure 3.6: Showing Study Workflow

Offshore hydrocarbon seepage and quantification approach dealt with mapping textural variations offshore that arise as a result of hydrocarbon seepages that

occur either on the water body. The band ratio normalized hydrocarbon index was used in mapping offshore seepages; the result was also quantified to map the extent and amount of water body alteration.

The columnar approach dealt with mapping columnar (non-textural) variations offshore and onshore that arise as a result of hydrocarbon activities in the test sites. The hydrocarbon activities include hydrocarbon flares, oil-tank farms (appendix I), oil terminals (appendix II) and oil exploration wells, these activities left signatures that alter the aerosol composition of the test sites. The methods employed in this approach were the SAM target detection and the image equalisation and k-means unsupervised cluster classification. The result of these methods defined the columnar hydrocarbon seepage mapping, and the results were quantified to map the extent and amount of aerosols alterations. The total hydrocarbon seepage map was defined by the overlay of results of the three approaches, and the total hydrocarbon seepage matrix was the adding up the quantification result of all three approaches.

3.1 METHODS

3.1.1 IMAGE UNMIXING

Linear spectral unmixing exploits the theory that the reflectance spectrum of any pixel is the result of linear combinations of the spectra of all endmembers inside that pixel (Adams et al,. 1986; Boardman, 1989). A linear combination in this context can be thought of as a weighted average, where each endmember weight is directly proportional to the area the pixel containing that endmember (Shippert, 2003). Linear Spectral Unmixing determines the relative abundances of materials that are depicted in multi- or hyper-spectral imagery based on the materials' spectral characteristics. The reflectance at each pixel of the image is assumed to be a linear combination of the reflectance of each material (or endmember) present within the pixel. For example, if 25% of a pixel contains material A, 25% of the pixel contains material B, and 50% of the pixel contains material C, the spectrum for that pixel is a weighted average of 0.25 times the spectrum of material A plus 0.25 times the spectrum of material B plus 0.5

times the spectrum of material C. So given the resulting spectrum (the input data) and the endmember spectra, the linear unmixing is solving for the abundance values of each endmember for every pixel. The number of endmembers must be less than the number of spectral bands and all of the endmembers in the image must be used. Spectral unmixing results are highly dependent on the input endmembers and changing the endmembers changes the results.

After a spectral and spatial browsing of the images coupled with the integration of other ancillary information regarding the geology of the area, 7 endmembers were chosen from mineral groups of carbonates, oxides, sulphate, sulphide and Phyllosilicate, table 3.2 describes the selected endmembers.

Table 3.2: Mineral endmembers selected from ASTER spectral library.

Mineral Group	**Minerals (SWIR)**
Carbonates	Calcite, Dolomite,
Oxides	Hematite
Sulphate	Alunite, Gypsum
Sulphide	Pyrite
Phyllosillicate	Kaolinite

Figure 3.7a shows the spectral plot of the mineral endmembers selected from ASTER spectral library (SWIR) and figure 3.7b shows the plot of the resampled endmembers. These endmembers were resampled to match the ASTER image reflectance, and also resampled using the ENVI spectral library resampling option to the ASTER SWIR band response reflectance (fig. 3.7b).

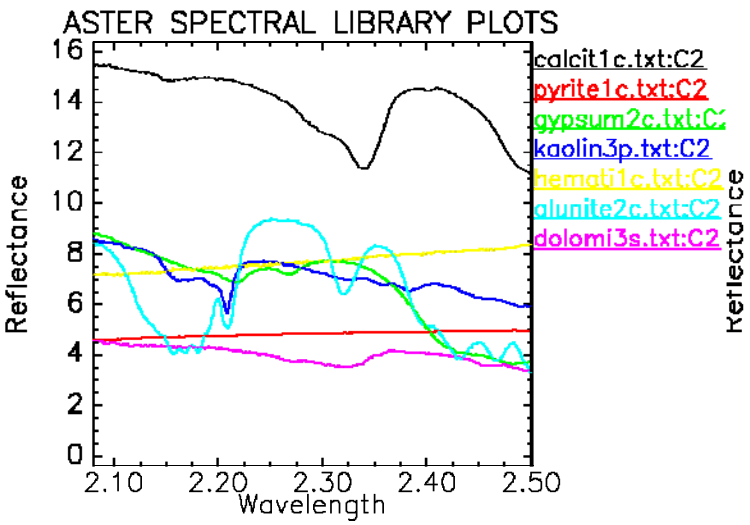

Figure 3.7a: ASTER spectral library plots of selected endmembers from the SWIR region

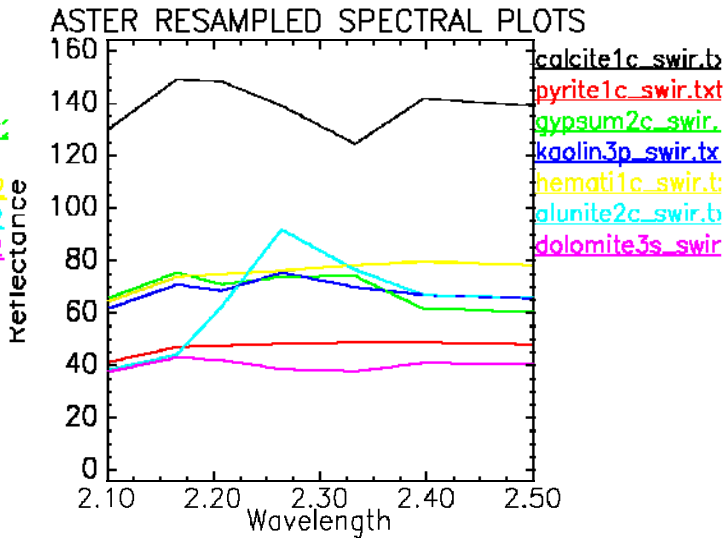

Figure 3.7b: ASTER spectral library plots of resampled selected endmembers from the SWIR region

3.1.2 PRINCIPAL COMPONENT ANALYSIS (PCA)

The principal components transformation is a multivariate statistical technique which selects uncorrelated linear combinations (eigenvector loadings) of variables in such a way that each successive extracted linear combination, or principal component (PC), has a smaller variance (Singh and Harrison, 1985). The statistical variance in multispectral images is related to the spectral response of various surficial materials such as rocks, soils and vegetation, and it is also influenced by the statistical dimensionality of the image data (Loughlin, 1991). Most of the variation of radiant spectral flux measured by a sensor depends on topographic shading and albedo effects at the surface. PCA is a powerful statistical technique that can be used for suppressing irradiance effects that dominate all bands, therefore enhancing spectral reflectance features of geological materials. PCA can be applied to multivariate datasets, such as multispectral remote sensing images, with the purpose of extracting specific spectral responses. Crosta and Moore (1989) developed a technique based on PCA for mapping iron oxide/hydroxides related to sulphide ore bodies in granite–greenstone belt terrains using Landsat TM. The technique, called 'feature-orientated principal component selection' (FPCS), relied on establishing the relationship between the spectral responses of target materials (ferric-oxide-rich soils) and numeric values extracted from the eigenvector

matrix used to calculate the principal component (PC) images. Using this relationship, they were able to determine which PCs contained the spectral information due to iron minerals and whether the digital numbers (DNs) of pixels containing the target materials had high (bright) or low (dark) values.

Loughlin (1991) modified the FPCS technique by selecting specific Landsat TM band sets and applying PCA separately to them, to ensure that certain materials (e.g. vegetation) would not be mapped and that spectral information due to target materials (alteration minerals) would be mapped into a single PC. The procedure proposed by Loughlin used Landsat TM band sets comprising bands 1, 3, 4 and 5 for deriving spectral information related to ferric oxides/hydroxides, which would be uniquely mapped into either PC3 or PC4. Another band set, comprising bands 1, 4, 5 and 7, was similarly used to derive information related to hydroxyl-bearing minerals and carbonates, also uniquely mapped into either PC3 or PC4.

This procedure, coined by Loughlin (1991) the 'Crosta technique', has been successfully used for mineral exploration purposes due to its ease of use and robustness (Bastianelli et al. 1993, Davidson et al. 1993, Ruiz-Armenta and Prol-Ledesma 1998, Souza Filho and Drury 1998, Tangestani and Moore 2001, 2002, Carranza and Hale 2002).

When multispectral images are treated as variables and subject to transformation, it follows that ordering of the principal components is influenced both by the spatial abundance of the various surficial materials and by the image statistics. Thus reducing the number of image bands input for PCA ensures that certain materials will not be mapped and increases the likelihood that others will be unequivocally mapped into one of the principal component images (Loughlin, 1991).

Principal component transform was applied to selected bands of the images and the PCA eigenvector loadings was examined to decide which of the principal component images will concentrate information directly related to the theoretical spectral signatures of specific targets. Louglin (1991) describes

the important of this method to include its ability to predict whether the target surface type is highlighted by dark or bright pixels in the relevant principal component image. PCA was applied to subsets of four ASTER bands -1, 4, 5, 6 using an adaptation of the Crosta technique proposed by Loughlin (1991) to map Al-OH bearing minerals. The subsets were selected according to the position of characteristic spectral features of key alteration mineral endmembers in the SWIR portions of the spectrum.

3.1.3 BAND RATIO – NORMALIZED HYDROCARBON INDEX

Previous studies have shown that spectral indices signatures of hydrocarbons are characterized by absorption features at 1.73 and 2.31µm (e.g. Clustis 1989, Ellis et al. 2000, Horig et al. 2001). Kuhn, F. et al. (2004) develop an hydrocarbon index for hysperspectral detection of hydrocarbons relying on the absorption features at 1.73 and 2.31µm. They aimed to develop an index that can be used similarly to the Normalized Difference Vegetation Index (NDVI), easy to use mathematical algorithm transforming multi-band data into a single band showing the presence of hydrocarbons. The uniqueness of this method is the selection of all pixels whose spectra contain the 1.73µm hydrocarbon feature.

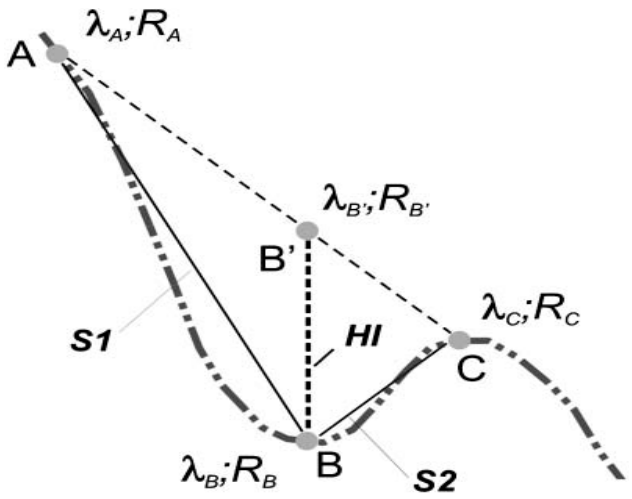

Figure 3.8: Enlarged 1.73µm portion of the spectral signature of hydrocarbon-bearing materials with 'index points' A, B, A' and C for the Hyrdocarbon Index; R_i and λ_i are the radiance values and the wavelength at the 'index points' (From Kuhn, et al. 2004).

Kuhn, F. et al. (2004) demonstrated that the hydrocarbon index uses the vertical line HI=BB' as indicator of the occurrence of oil and other

hydrocarbons within the pixel. If hydrocarbon-bearing materials are present at the ground surface, the index points A, B, and C forms a triangle (HIw0). As an approximation, it can be assumed that the larger the HI value, the larger the hydrocarbon concentration. If no hydrocarbon-bearing material is present, the index points A, B, and C lie along a nearly straight line, and no triangle is formed (HI~0). The Hydrocarbon Index can be calculated as follows:

$$HI = (\lambda_B - \lambda_A)\frac{R_C - R_A}{\lambda_C - \lambda_A} + R_A - R_B$$

Where R_A; λ_A, R_B; λ_B and R_C; λ_C are radiance/wavelength pairs for each index point (fig. 3.8).

They calculated the hydrocarbon index as follows: -

$$HI = \frac{2}{3}(R1741 - R1705) + R1705 - R1729$$

Or $$HI = 2(b_3 - b_1)/3 + b_1 - b_2$$

Where b1 is swir1 band 1705, b2 is swir1 band 1729 and b3 1741nm of the HyMap radiance image. This equation was adapted for ASTER sensor used for this study to have a normalized hydrocarbon index as follows:

$$HI = 2(b_8 - b_5)/3 + b_5 - b_6$$

Where b6 is SWIR band 5 - 2.165µm, b8 is SWIR band 6 – 2.205µm and b8 is SWIR band 8 – 2.327µm.

3.1.4 SAM TARGET DETECTION

The SAM Target Finder with BandMax wizard is implemented in ENVI 4.1 software, the wizard is used to find target with the Spectral Angle Mapper (SAM) classification and Bandmax algorithm. The Spectral Angle Mapper (SAM) computes a spectral angle between each pixel spectrum and each target spectrum, the smaller the angle the more similar the pixel and the target spectra (Yuhas et al., 1992). This spectral angle will be relatively insensitive to changes in pixel illumination because increasing or decreasing illumination do

not change the direction of the vector, only its magnitude (Shippert, 2003). The wizard leads through the process of finding targets in images. The BandMax part of the wizard increases classification accuracy by determining an optimal subset of bands to ease target separation from known backgrounds materials (ENVI Users Guide 4.1).

The wizards allow the selection of target and background the target might be embedded as endmembers. It also allows the selection of the SAM maximum Angle Threshold for SAM classification of the images as per target abundance.

In the study, this wizard was used to map and classify the abundance of the Hydrocarbon flares, halos and oil-tank farm through out the images. A flare pixel and oil- farm tank pixel was chosen as the target endmembers while water, cloud, land and other unknown material were chosen as background endmembers.

3.1.5 IMAGE EQUALIZATION AND K-MEANS CLUSTER CLASSIFICATION

This is entirely a pixel based approach to map all flares pixels and this indirectly map the flare pattern and direction when integrated with wind speed and direction. Flare pixels were much depicted in the Shortwave Infrared (SWIR) band 6, the image equalization stretching was applied to the images to expose pixels similar to that of the flares. K-means classification was then applied to SWIR band 6 and the all flare-like pixels were mapped out. The strength of the method is that k-means classification calculates initial class means evenly distributed in the data space and then interactively clusters the pixels into the nearest class using a minmum distance technique (Envi Users Guide 4.1). Each iteration recalculates class means and reclassifies pixels with respect to the new mean. All pixels are classified to the nearest class unless a standard deviation or distance threshold is specified, in which case some pixels may be unclassified if they do not meet the selected criteria. The process continues until the number of pixels in each class changes by less than threshold or the maximum number of iterations is reached.

CHAPTER FOUR

4.0 RESULTS

The results of the study are structured in three groups, each representing the mapping approach adopted in the study. Onshore hydrocarbon seepage mapping entails examining results of linear unmixing and Principal Component Analysis (PCA) implementations; offshore hydrocarbon seepage mapping consists of result of normalized hydrocarbon index implementation; columnar hydrocarbon seepage mapping is defined by the results of both SAM target detection and image equalization with k-means classification. All methods were applied to both test sites (images). The final hydrocarbon seepage map of the Niger delta is defined by the overlay of all described results.

4.0.1 IMAGE UNMIXING

Image unmixing was applied on the two test sites. The endmembers abundance was mapped as shown in the figure below (fig. 4.1a and 4.2b). The dolomite mineral was mainly noticed on the shorelines (fig 4.1a), suggesting that dolomite make up the primary constituent of the beach sands in test site I.

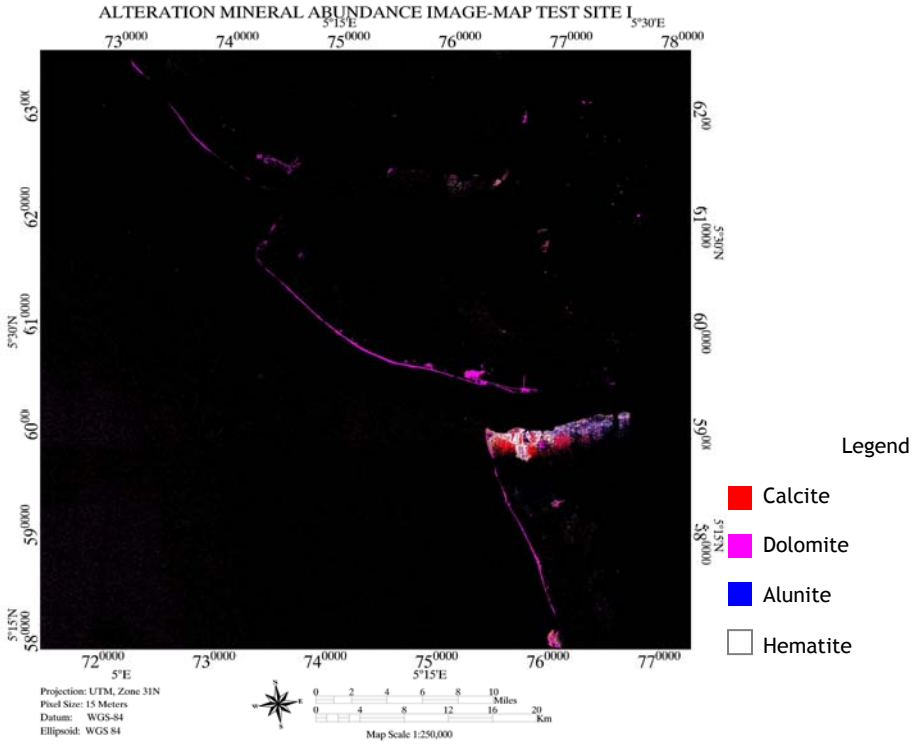

Figure 4.1a: showing alteration mineral abundance test site I

It is suggested that ASTER SWIR band passes identifies classes of mineral assemblages (table 3.1); to narrow down the percentage of false classification, the endmembers were re-class as per mineral groups and the unmixing perform to the two test sites again. The endmembers abundance (mineral group) was successfully mapped for test site I and II (fig.4.1b and 4.2b).

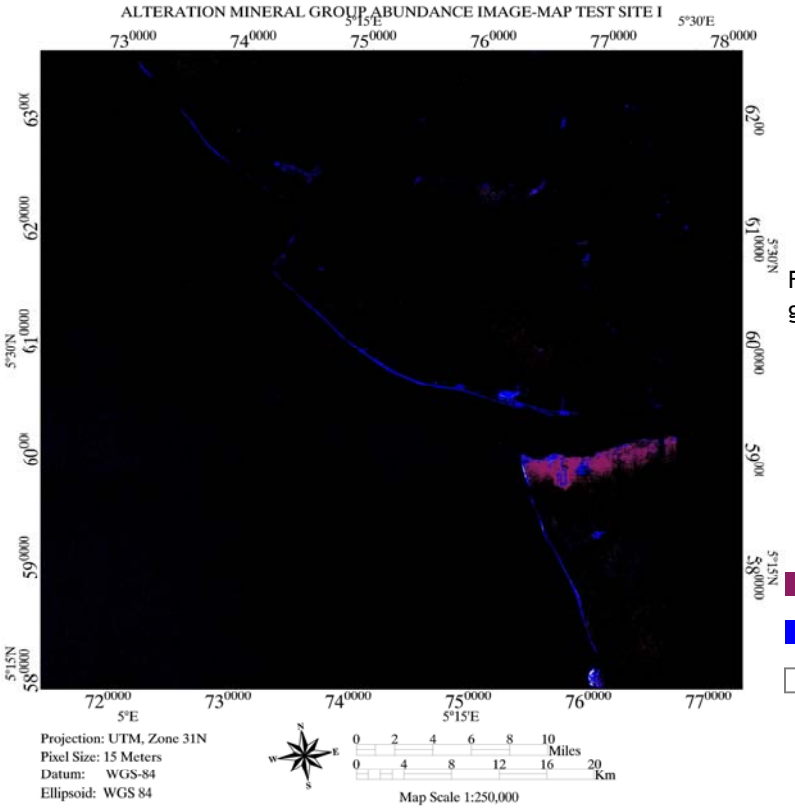

Figure 4.1b: showing alteration mineral group abundance test site I

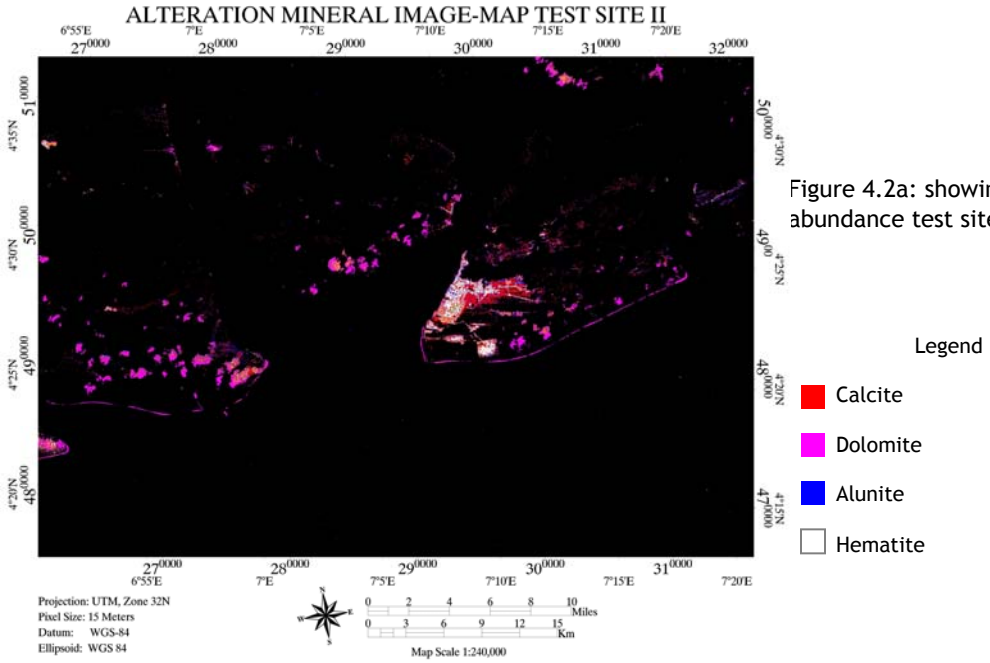

Figure 4.2a: showing alteration mineral abundance test site II

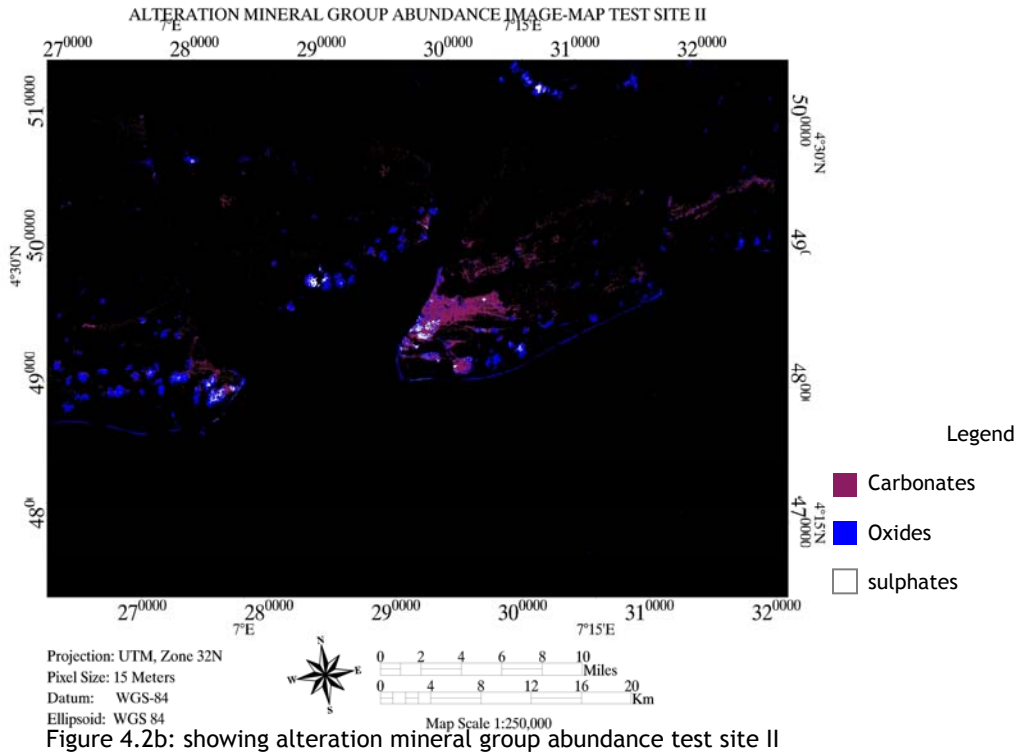

Figure 4.2b: showing alteration mineral group abundance test site II

4.0.2 PRINCIPAL COMPONENT ANALYSIS

ASTER bands 1, 4, 5, 6 were selected to map Al-OH bearing minerals; tale 4.1 shows the eigenvector bands statistics.

Table 4.1: Eigenvector statistics for ASTER band 1, 4, 5 and 6. These band set was selected for identifying spectral response from Al-OH bearing minerals.

	PC1	PC2	PC3	PC4
Band 1	0.700867	0.704100	-0.113743	-0.009547
Band 4	0.513372	-0.608898	-0.598883	-0.083858
Band 5	0.343983	-0.259278	0.448852	0.782932
Band 6	0.356245	-0.257414	0.653402	-0.616355

Table 4.1 describes the principal components transformation on ASTER bands 1, 4, 5 and 6 for test site I. The PCs can be interpreted as albedo in PC1, VNIR vs SWIR in PC2, partly vegetation in pc3, Al-OH as dark pixels in PC4. This Al-OH image is reproduced in figure 4.3a.

Table 4.2: Eigenvector statistics for ASTER band 1, 4, 5 and 6, test site II

	PC1	PC2	PC3	PC4
Band 1	0.343359	0.916078	-0.207077	-0.004881
Band 4	0.709096	-0.397156	0.579853	-0.056751
Band 5	0.414860	-0.046717	-0.462788	0.782008
Band 6	0.455169	-0.029751	-0.637743	-0.620660

For test site II, table 4 describes similar principal component and PC4 maps Al-OH as dark pixels (green colour in this case- Fig. 4.3b).

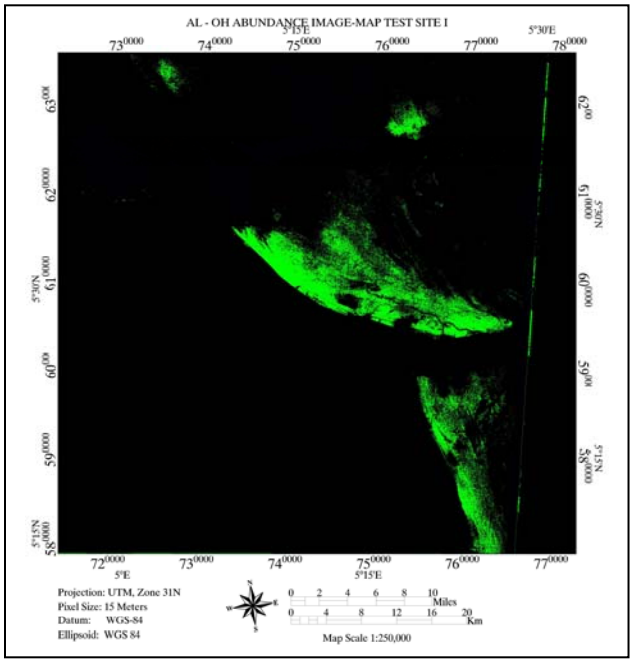

Figure 4.3a: showing AL-OH mineral abundance test site I

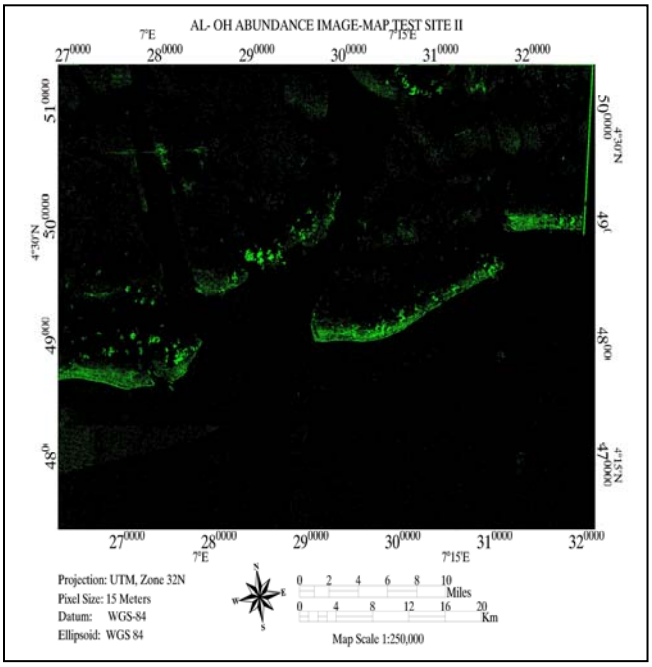

Figure 4.3b: showing AL-OH mineral abundance test site II

4.0.3 BAND RATIO – NORMALIZED HYDROCARBON INDEX

The normalized index equation was adapted for ASTER sensor used for this study and was applied to both test sites. Figures 4.4a and b shows the result of band ratio applied to both test sites. The spatial distribution of the band index result was based offshore; this could be due to the almost homogenous nature of the water body. Few onshore pixels were mapped with this method, this onshore pixels were those associated with oil activities like terminals and oil

tank-farm around the area. Such pixels could indicate source of the seepages to the offshore area.

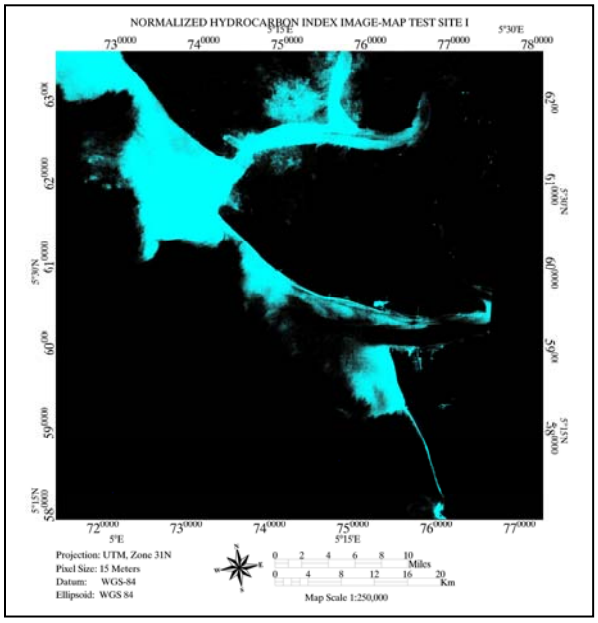

Figure 4.4a: Band ratio index results test site I

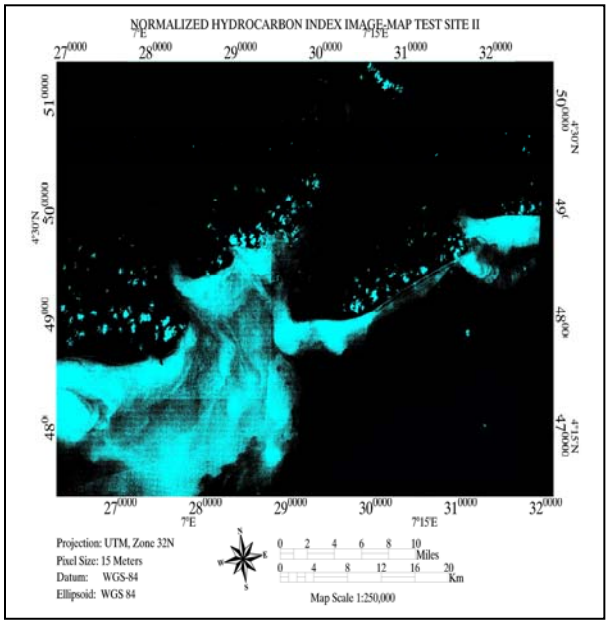

Figure 4.4b: Band ratio index results test site II

4.0.4 SAM TARGET DETECTION

As described in the methods, the SAM target detection was applied to both sites to map targets associated to hydrocarbon activities – oil tank farm, hydrocarbon flares, oil terminals; the following results were gotten (fig. 4.5a and b) for test sites I and II.

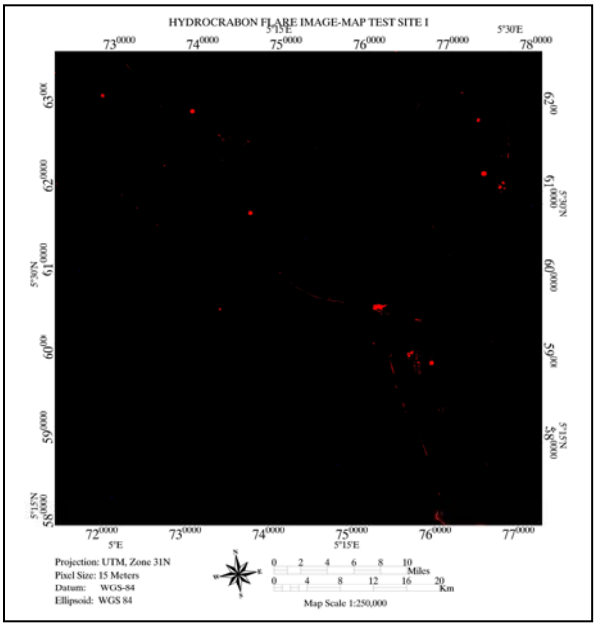

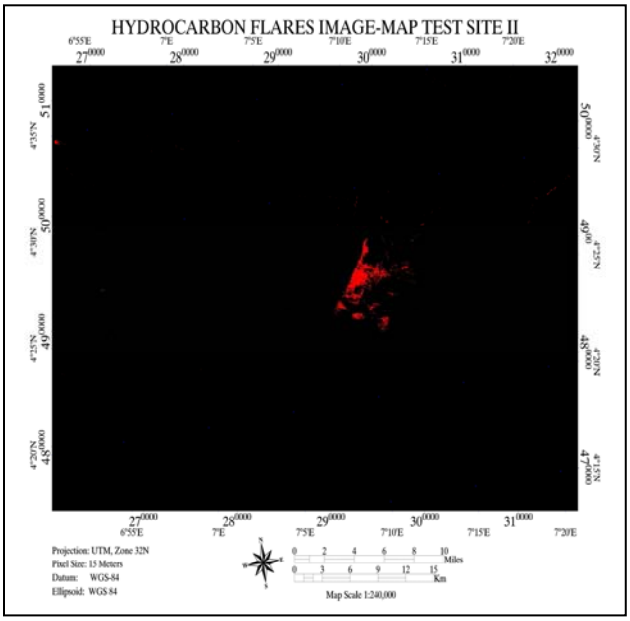

Figure 4.5a and b: SAM target finder results- maps hydrocarbon flares, oil farm-tank and oil terminals test site I and II

4.0.5 IMAGE EQUALIZATION AND K-MEANS CLUSTER CLASSIFICATION

This method was applied to both test sites to map pixels patterns associated with the observed hydrocarbon flares; the following results were gotten (Fig. 4.6) for test site I (see appendix V for a zoomed-in image map showing flares and associated flares pixels – mapping the extent of the flares in test site I).

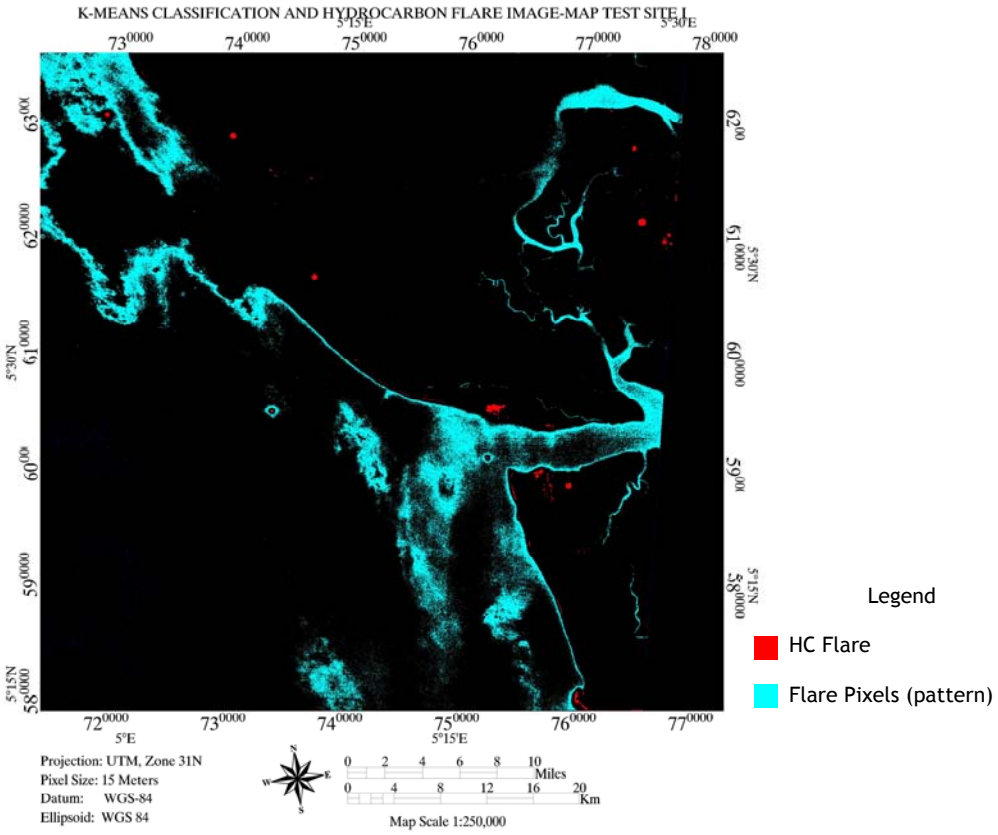

Figure 4.6: K-means classification results- maps pixels associated with hydrocarbon flares test site I.

4.0.6 ONSHORE HYDROCARBON SEEPAGE MAPPING

The image unmixing and Principal Component Analysis (PCA) maps the abundance of the alteration zone mainly carbonates oxides and sulfates. In both test sites, a greater percentage of the map area were close to the shore as seen in the figure below (fig.4.7a and b) and the remaining were onshore. These two methods were effective in mapping onshore hydrocarbon induced alterations. Table 4.3a &b – 4.5a&b, describes the pixels and percentage area mapped with these methods.

For test site I with a total of 20,926,000 pixels, table 4 summarize the quantification of each abundance mineral or group.

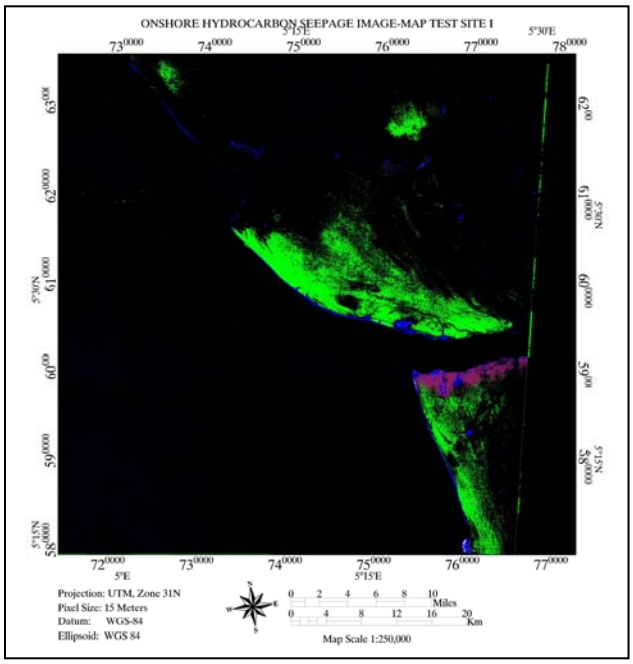

Figure 4.7a: Onshore hydrocarbon seepage map-results of Image unmixing with PCA for test site I

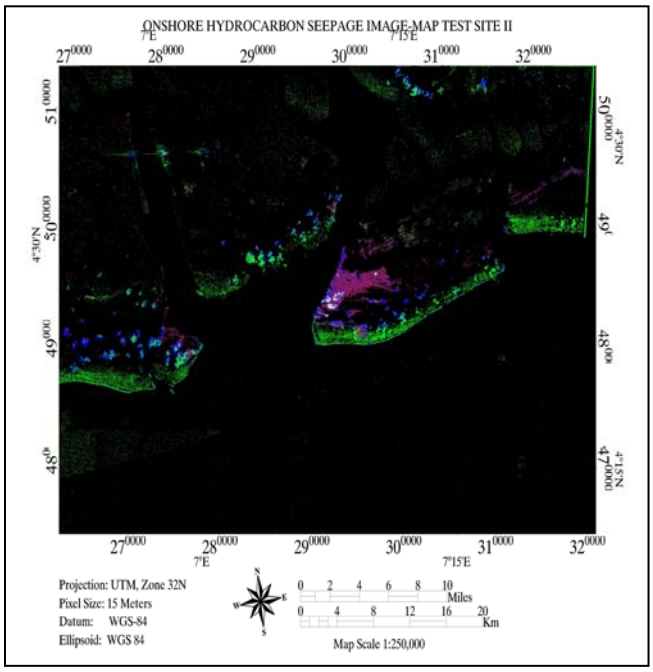

Figure 4.7b: Onshore hydrocarbon seepage map-results of Image unmixing with PCA for test site II

Table 4.3a and b: Quantification of the onshore hydrocarbon seepage map of test site I for carbonates and oxides mineral group.

Carbonates	No. of Pixels	percentage	Area (m^2)
Calcite	29,734	0.1422	6690150
Dolomite	16,598	0.0794	3734550

Oxides	No. of Pixels	percentage	Area (m^2)
Hematite	1,677	0.0080	377325
Magnetite	1	0.0000	225

The carbonates mineral group total 46,332 pixels was about 0.22 percent of the total pixels in the area. The spatial distribution of the carbonates mineral group was close to already existing hydrocarbon infrastructures (oil-tank farm, oil terminals, etc.) and partly distributed within the test sites. Because of the closeness of the map carbonates mineral to hydrocarbon infrastructures, it

would be safe to assume that a majority of the mapped carbonate mineral could be due to seepages cause by reworked hydrocarbon. Other areas far of hydrocarbon infrastructure could be as result of reworked hydrocarbon in the past or there is actually induced hydrocarbon seepage at those points. The total area covered by carbonates mineral is about 10424700m^2. Diagenetic carbonates in the form of Cemented calcite are common in areas of petroleum fields (Schumacher, 1996). For the oxide mineral group, only hematite was mapped as an alteration mineral in test site 1. A total number of 1677 pixels were mapped as hematite, 0.008 percent of the total pixels and area of 377325m^2. A good percent of mapped hematite was distributed around the hydrocarbon flares and others on the shoreline. Hematite has been found to a key constituent in bleaching of red beds, bleaching of red beds occurs whenever acidic or reducing conditions also favour ferric oxide (hematite), (Schumacher, 1996). Areas mapped as hematite could signify areas of bleached red beds.

Table 4.4a and b: Quantification of the onshore hydrocarbon seepage map of test site I for Sulphates, Sulphides and AL-OH mineral group test site I.

Sulphates	No. of Pixels	percentage	Area (m^2)
Alunite	247	0.0012	55575
Gypsum	217	0.0010	48825
AL-OH Group	1040895	4.9765	234201375

Sulphides	No. of Pixels	percentage	Area (m^2)
Pyrite	4	0.0000	900
Physiosillicates			
Kaolinite	5	0.0000	1125

The Sulphate mineral groups accounted for about 264 pixels and 0.0022 percent of test site I. The spatial distribution was not particularly defined, but a good percent was on the shoreline and scantily on the water body. Gypsum occurrence is known to be one of the products of early hydrocarbon seepages onshore. Schumacher (1996) noted that gypsum, jarosite and sulphur are the common alteration products found in Persia as result of the interaction of petroleum with evaporates. Other causes could be responsible for the occurrences of sulphate mineral, but since the test site is in a hydrocarbon active environment such possibility is low.

The sulphide mineral group particularly pyrite is notice in many petroleum fields worldwide (Schumacher, 1999). The formation of secondary pyrite and other sulfides has been documented for many petroleum fields (Huges et al., 1986). Pyrite is the dominant sulphide mineral in most hydrocarbon induced alterations zones, but pyrrhotite, marcasite, galena and native sulphur are also found and may be locally abundant (Schumacher, 1996). Pyrite can be precipitated in a reducing environment, given a source of sulfur and iron. The major source of sulfur in a petroleum province is hydrogen sulphide gas from the petroleum itself, from anaerobic bacterial activity, or from the oxidation of petroleum in the near surface (Schumacher, 1996), this justifies the present of sulphide mineral group in test site I. Mapped pyrite only cover about 900m^2, in test site I, but in test site II, mapped pyrite was much higher.

The production of CO2, H2S, and organic acids resulting from the microbial oxidation of hydrocarbons in nearsurface soils and sediments can create reducing, slightly acidic conditions that promote the diagenetic weathering of feldspars to produce clays and may lead to the conversion of normally stable illitic clays to kaolinite. Clays thus formed remain chemically stable unless their environment is changed (Schumacher, 1996). Kaolinite in the study area covered an area of 1125m^2.

Al-OH mineral group accounted for about 4.9 percent of test site I, this mineral group are made of Muscovite-Montmorillonite-illite-Al smectite. Its occurrence

has been found to be inversely related to that of kaolinite, suggesting that the enrichment of any of them is related to the depletion of the other.

Table 4.5 a& b: describes quantification for test site II, Carbonates and Oxide mineral group.

Carbonates	No. of Pixels	percentage	Area (m^2)
Calcite	51,300	0.4337	11542500
Dolomite	24,248	0.2050	5455800

Oxides	No. of Pixels	percentage	Area (m^2)
Hematite	13,704	0.1159	3083400
Magnetite	100	0.0008	22500

For test site II, the spatial distribution of the mapped alteration minerals were similar, only that the sulphate mineral group were not mapped in this test site. This could be probably due to the large ratio of water body to the land (onshore). This method was only effective in mapping onshore hydrocarbon induced seepages.

Table 4.5 a & b: describes quantification for test site II, Sulphides, Sulphates and AL-OH mineral group.

Sulphates	No. of Pixels	percentage	Area (m^2)
Alunite	0	0	0
Gypsum	0	0	0
AL-OH Group	257,082	2.1734	57843450

Sulphides	No. of Pixels	percentage	Area (m^2)
Pyrite	64	0.0005	14400
Physiosillicates			
Kaolinite	8	0.0000	1800

4.0.7 OFFSHORE HYDROCARBON SEEPAGE MAPPING AND QUANTIFICATION

The normalized band ratio already discussed in the previous chapter was effective in mapping offshore seepage alterations. This was possible considering the almost homogenous nature of the water body. Onshore hydrocarbon induced variations were also mapped with this method but mapped onshore alterations were on the shoreline or close to known hydrocarbon installations (see figures 4.6a&b). Arguably, it follows that the source of the offshore pollution (variation) would be the mapped onshore pixels. Mapped offshore hydrocarbon alterations could have been transported during flooding or shoreline erosions or even during oil activities at the terminals to the water body. Table 4.6 describes the quantification of mapped offshore hydrocarbon seepages at both test sites.

Table 4.6: describes quantification of the Offshore Hydrocarbon seepages approach results.

Test site	No. of Pixels	percentage	Area (m^2)
I	2257673	10.7939	507976425
II	2960557	25.02	666125325

4.0.8 HYDROCARBON COLUMNAR SEEPAGE MAPPING

The result of the SAM target finder and that of the image equalization with k-means unsupervised classification together mapped the columnar hydrocarbon seepages. The SAM target finder was used to find the abundance of the hydrocarbon flares through both test sites. These flares were the source of the columnar hydrocarbon seepages mapped with the image equalization and k-means unsupervised classification. This method was effective over the water body possibly due to the almost homogenous nature of the water (fig 4.8). The average wind speed and direction on the same day the images of both test sites were acquired was very useful in the study. The idea behind this approach was to trace and account for the source of the columnar seepages; the closer a

cloud of hydrocarbon seepage is to a flare and in direction of the wind, then the flare is responsible for such hydrocarbon cloud.

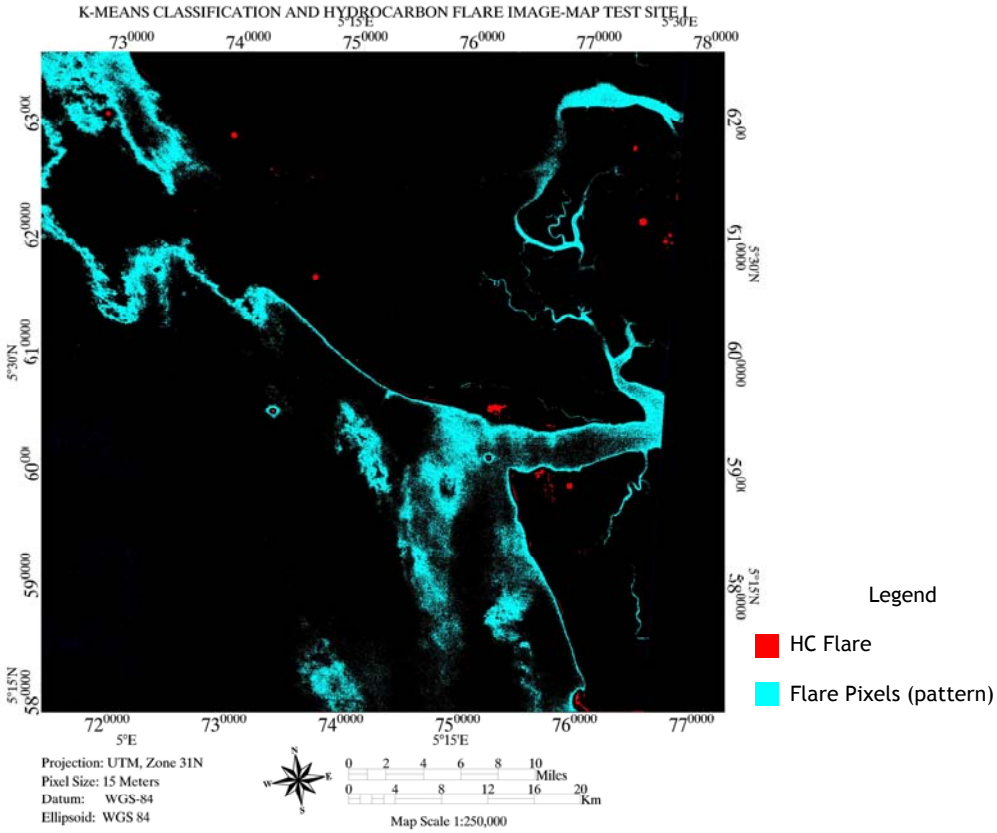

Figure 4.8: K-means classification results- maps pixels associated with hydrocarbon flares test site I.

For test site I, the wind speed was about 4m/s (appendix III) and in direction of 270^0 in the northwesterly direction. This accounted for some seepage clouds mapped in this direction (figure 4.8). The total number of pixel mapped as hydrocarbon flare was about 60,805 representing 0.291% of the total area. This shows that test site I is hydrocarbon active area.

4.0.9 TOTAL HYDROCARBON SEEPAGE MAP AND SEEPAGE MATRIX

The total hydrocarbon seepage map was defined by an overlay of the results of the three approaches used in this study; the approaches include: -

I. Onshore Seepage Mapping: this includes generalized hydrocarbon alteration zones and the onshore Al-OH mineral group.

II. The offshore seepage mapping: this was define by the normalized hydrocarbon index, this method as described earlier was effective in mapping surface hydrocarbon induced variations on the water almost homogenous body.

III. The columnar seepage mapping: here the wind speed was useful in attributing seepage clouds to different mapped flares in the study area.

With these three approaches all surface and columnar variations both onshore and offshore was mapped and accounted for in the test sites (fig.4.9).

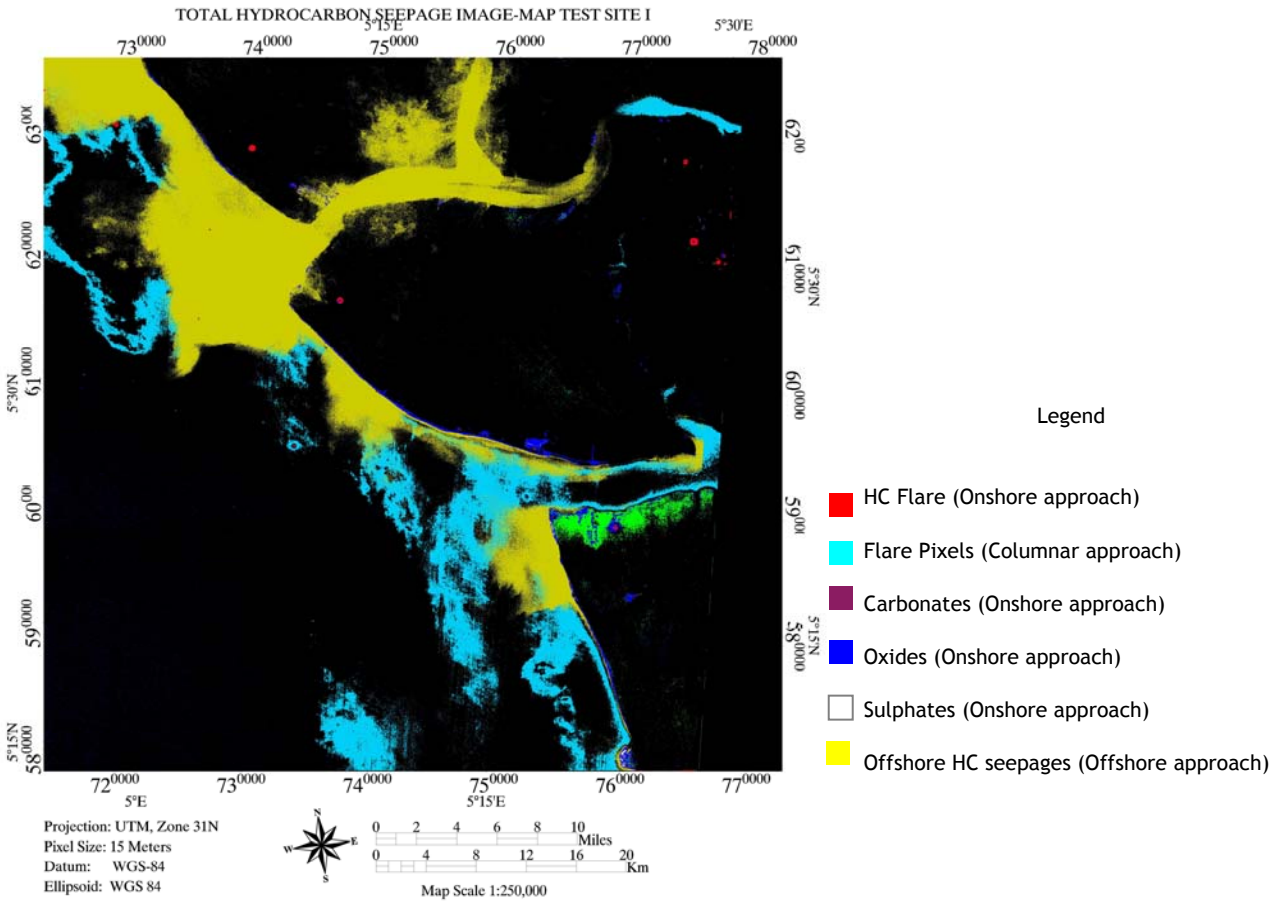

Figure 4.9a: Hydrocarbon seepage map of study area I

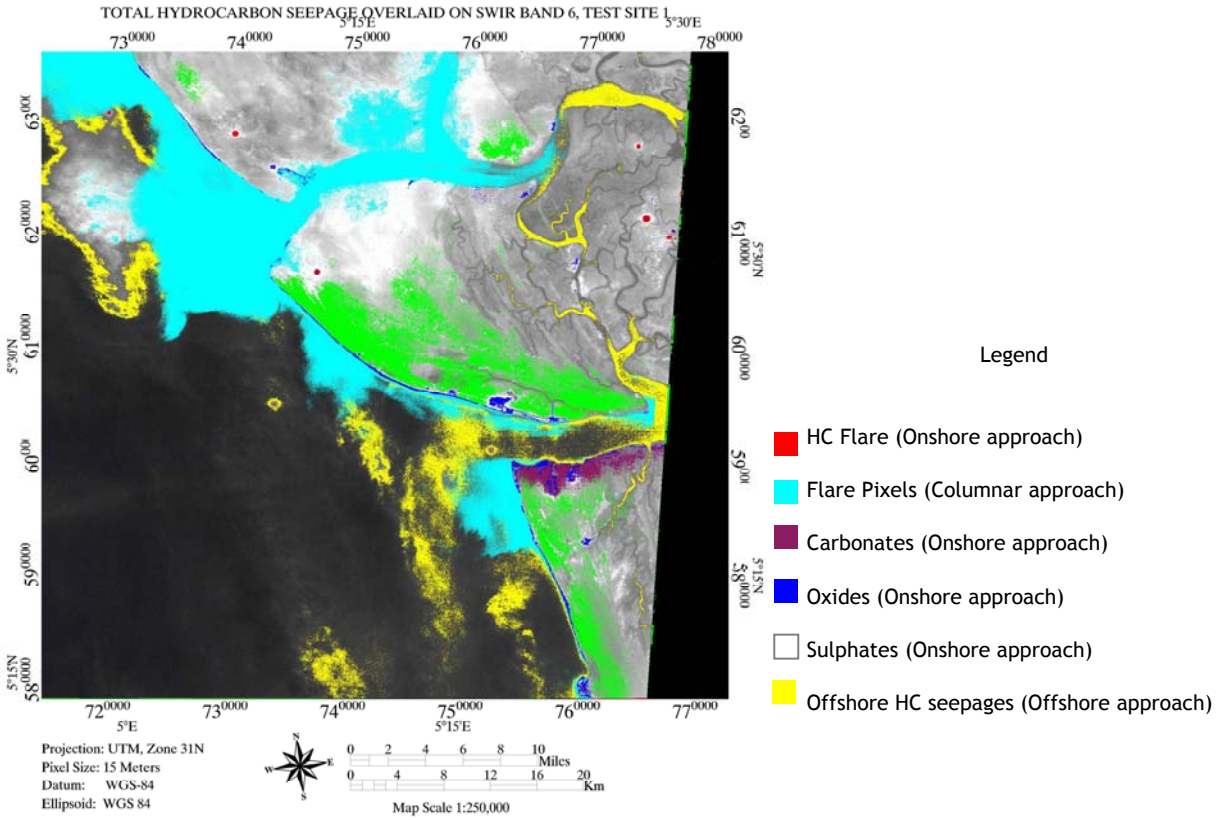

Figure 4.9b: Hydrocarbon seepage map of study area I overlaid on SWIR band 6.

4.0.9.1 TEST SITE I HYDROCARBON SEEPAGE MATRIX

Table 4.7 describes the hydrocarbon seepage matrix with test site I – Onshore, Offshore and columnar quantification

Location	No. of Pixels	percentage	Area (m^2)
Onshore	1089378	5.2083	245110050
Offshore	2257673	10.7939	507976425
Columnar	60805	0.291	13681125

From the table (table 4.7), possible hydrocarbon seepages was greatly detected offshore (water body) this could be partly due to the almost homogenous nature and could also real sense be the location where hydrocarbon seepages was greatest in test site I.

For test site II, fig 4.9 c&d shows the total hydrocarbon seepage map of test site II.

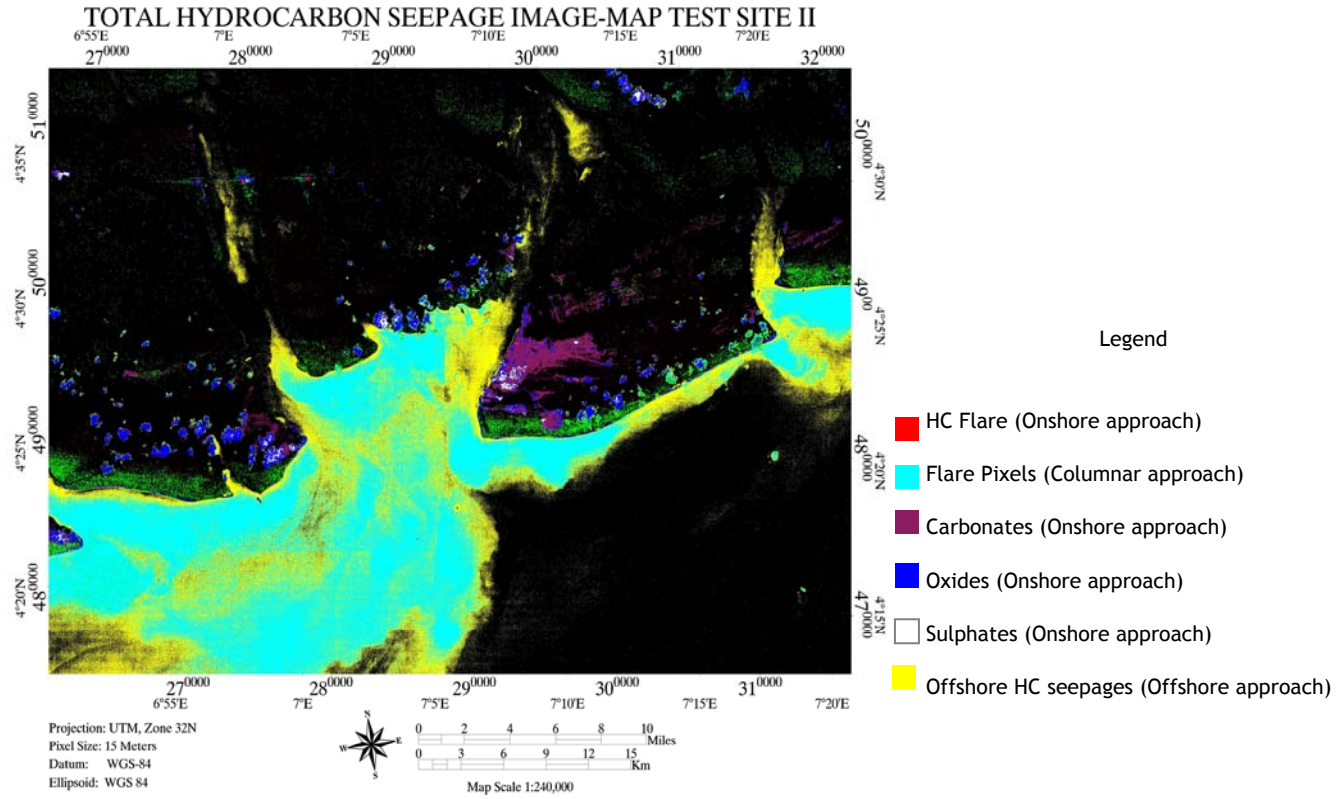

Figure 4.9c: Hydrocarbon seepage map of study area II

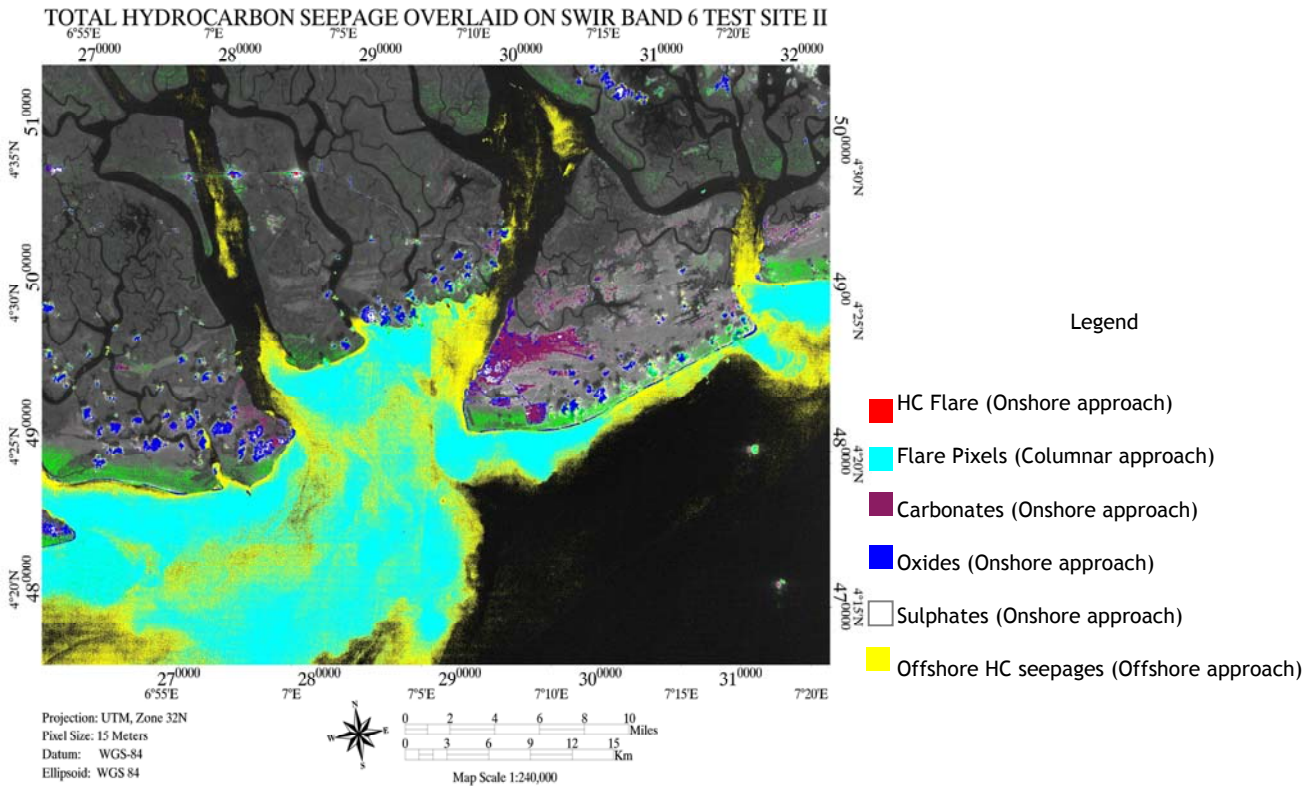

Figure 4.9d: Hydrocarbon seepage map of study area II overlaid on SWIR band 6

4.0.9.2 TEST SITE II HYDROCARBON SEEPAGE MATRIX

Table 4.8 describes the hydrocarbon seepage matrix for test site I – Onshore, Offshore and columnar quantification

Location	No. of Pixels	percentage	Area (m^2)
Onshore	346506	2.9293	77963850
Offshore	2960557	25.02	666125325
Columnar	691310	5.8445	155544750

From table 4.8 above, out a total of 11828328, offshore portion of test site II is more affected by hydrocarbon seepages and like test site I, this area has the most mapped seepages.

With the implemented three approaches, the study provides insight to the study research questions.

4.0.9.3 PROBLEMATIC PIXELS

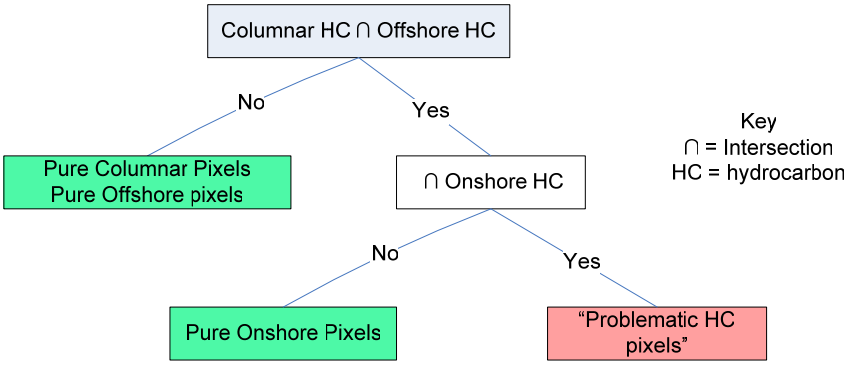

Figure 4.9e: ENVI Decision Tree parameters used to isolate "problematic pixels".

Pixels that were together mapped in more than one approach were called the "problematic pixels". These pixels are overlaps (intersection) of different approach results within the overlay results. To accurately quantify the result of the different approach ENVI classification decision tree was used to separate

the problematic pixels with "pure" pixels. Figure 4.9 e, shows the decision tree parameters as it was being used for this purpose.

Table 4.8 describes the actual hydrocarbon seepage matrix minus the isolated "problematic pixels test site I

	Onshore	Offshore	Columnar	Actual Area (m^2)
Onshore	1070158	10468	8752	240785550
Offshore	10468	22163946	40259	4986887850
Columnar	8752	40259	11794	2653650

Table 4.9 describes the actual hydrocarbon seepage matrix minus the isolated "problematic pixels test site II

	Onshore	Offshore	Columnar	Actual Area (m^2)
Onshore	346506	0	0	77963850
Offshore	0	2553715	406842	574585875
Columnar	0	406842	284468	64005300

The columnar hydrocarbon seepage mapping approach results was intersected with that of the offshore and the result of the intersection, intersected with the onshore approach result. Pixels that fall within the intersection were the problematic pixels while others were pure pixels with respect to mapping approach type. The decision tree based classification was applied to both test sites and the statistics of the resulting images was calculated and this defines the actual quantification of the result of the different approaches, (table 4.8 and 4.9) this way the "problematic pixels" were isolated during the quantification. The problematic pixels that were onshore and also associated with the columnar and offshore hydrocarbon seepages in test site I were pixels that indicate the source of hydrocarbon seepages mapped offshore as columnar and offshore hydrocarbon seepages.

CHAPTER FIVE

5.0 CONCLUSIONS AND RECOMMENDATIONS

5.1 CONCLUSIONS

This study shows that ASTER products particularly the SWIR image can be successfully used in mapping hydrocarbon seepages or hydrocarbon-induced alterations exposed the surface. The three approaches adopted for this study; onshore, offshore and columnar were able to map hydrocarbon induced alterations or seepages. Onshore method is defined by result of linear unmixing and Principal Component Analysis (PCA), offshore method is defined by the result of the normalized hydrocarbon index and the columnar hydrocarbon seepages is defined by the result of image equalization with a k-means classification. With all three approach the spatial extent and approximate pixel-based quantity of hydrocarbon induced alterations and seepages was accounted for

Mapped alteration minerals with the onshore mapping approach has been proven from past work to be directly or indirect related to an hydrocarbon induced alterations or seepages in similar petroleum environments. Arguably, the greatest portion of hydrocarbon induced alterations and seepages were mapped offshore; this could be due to the almost homogeneous nature of the water body at both test sites. The detected hydrocarbon flares was the major source of columnar hydrocarbon seepages. Average wind speed and direction of the same day images of the test sites were acquired was used to allocate hydrocarbon cloud to its possible source; the closer a columnar hydrocarbon cloud is to a hydrocarbon flare and in the direction of the wind, the higher the likelihood that such flare is the source of the hydrocarbon cloud.

5.2 RECOMMENDATIONS

Listed here are potential areas which were not explored during this study and might need further research.

I. To explore the potential of ASTER TIR image acquired at night in detecting hydrocarbon flares and some hydrocarbon seepage pattern in areas with similar petroleum setting.

II. To apply the three methods in an area with little or no active petroleum activity going on, to test the robustness of the methods employed.

III. Apply the methods in a test sites were all the petroleum system has been accounted for to test the robustness of these methods.

IV. An exhaustive fieldwork would help account and better validate results gotten from this methods; this would include sampling of the atmosphere around the study area to detect key components and proportions, thus validating the columnar method.

V. These methods should also be experimented with other hyperspectral and multispectral sensors.

REFERENCE CITED

Adams, J. B., Smith, M. O., and Johnson, P.E. (1986): Spectral mixture modeling: A new analysis of rock and soil types at the Viking Lander 1 site. Journal of Geophysical Research, vol. 91(B8), pp. 8090-8112.

Almeida-Filho, R., Miranda, P., Yamakawa, T. (1999): Remote Detection of a Tonal Anomaly in an Area of Hydrocarbon Microseepage, Tucano Basin, North-Eastern Brazil. Internal Journal of Remote Sensing, 1999, Vol.20, No. 13, pp.2684-2688.

Almeida-Filho, R. (2002): Remote Detection of Hydrocarbon Microseepage-Induced Soil Alteration. International Journal of Remote Sensing, 2002, Vol. 23, No. 18, pp. 3523-3524

ASTER Global Viewer. Access September 8 (2004): from http://asterweb.jpl.nasa.gov/glovis.asp.

BASTIANELLI, L., BELA, G. D., and TARSI, L., 1993, Alteration mapping: a case study in mid-south Bolivia. Proceedings of the 9th Thematic Conference on Geologic Remote Sensing, Pasadena, CA (Ann Arbor, MI: Environmental Research Institute of Michigan), pp. 1133–1144.

Boardman, J. W. (1989): Inversion of imaging spectrometry data using singular value decomposition. Proceedings of the Twelfth Canadian Symposium on Remote Sensing, v. 4., pp. 2069-2072.

Brownfield, Michael E., Charpentier, Ronald R., Tuttle, Michele L. W. (1999): The Niger Delta Petroleum System: Niger Delta Province, Nigeria, Cameroon, and Equatorial Guinea, Africa, Open-File Report 99-50-H, United state Geological survey (USGS) Denver, Colorado.

CARRANZA, E. J. M., and HALE, M., 2002, Mineral imaging with Landsat Thematic Mapper data for hydrothermal alteration mapping in heavily vegetated terrain. International Journal of Remote Sensing, 23, 4827–4852.

Clutis, E. A. (1989): Spectral Reflectance Properties of Hydrocarbons: Remote-Sensing Implications. Science 245, p 165-168

CROSTA, A. P., and MOORE, J. MCM., 1989, Enhancement of Landsat Thematic Mapper imagery for residual soil mapping in SW Minas Gerais State Brazil: a prospecting case history in greenstone belt terrain. Proceedings of the 9th Thematic Conference on Remote Sensing for Exploration Geology, Calgary (Ann Arbor, MI: Environmental Research Institute of Michigan), pp. 1173–1187.

Crosta, A. P., and de Souza Filho, C. R. (1997): Evaluating AVIRIS hyperspectral remote sensing data for geological mapping in laterized terrains, central Brazil: in Proceedings of the 12th International Conference Applied Geologic Remote Sensing, Environmental Research Institute of Michigan, Ann Arbor, Mich, p. II-430 – 437.

DAVIDSON, D., BRUCE, B., and JONES, D., 1993, Operational remote sensing mineral exploration in a semi-arid environment: the Troodos Massif, Cyprus. Proceedings of the 9th Thematic Conference on Remote Sensing for Exploration Geology, Pasadena, CA (Ann Arbor, MI: Environmental Research Institute of Michigan), pp. 845–859.

De Jong, S., Van der Meer, F. (2002): Chapter 2: Basic Analytical Techniques, in Imaging Spectrometry: Basic Principles and applications, edited by Freek D. van der Meer and Steven M. de Jong (Kluwer Academic Publishers) p 17-64

Donovan, T. J. (1974): Petroleum microseepage at Cement, Oklhoma – evidence and mechanisms: AAPG Bulletin, v. 58, p.429-446

Donovan, T. J., Forgey, J. and Roberts, A. (1979): Aeromagnetic detection of diagenetic magnetite over oil fields: AAPG Bulletin, v. 63, p.245-248

Doust, H., and Omatsola, E. (1990): Niger Delta, *in*, Edwards, J. D., and Santogrossi, P.A., eds., Divergent/passive Margin Basins, AAPG Memoir 48: Tulsa, American Association of Petroleum Geologists, p. 239-248.

ENVI 4.0 Tutorial 19. (2003): Geologic Hyperspectral Analysis Case History, September Edition, Research systems Incorporated, p 439-448

Earth Observing system (EOS). Accessed September, 12 2004, from http://edcimswww.cr.usgs.gov/pub/imswelcome/

Ellis, J. M., David, H. H. and Quinn, M., B. (2000): Airborne hyperspectral imagery for the petroleum industry. Proceedings of the 14th International Conference on Applied Geologic Remote Sensing, Las Vegas, Nevada, 6-8 November 2000, p.89-96.

ENVI User's Guide 4.1. Research System, Inc., 2004

Ejedawe, J.E. (1981): Patterns of incidence of oil reserves in Niger Delta Basin: American Association of Petroleum Geologists, v. 65, p. 1574-1585.

Ekweozor, C. M., and Daukoru, E.M (1984): Petroleum source bed evaluation of Tertiary Niger Delta--reply: American Association of Petroleum Geologists Bulletin, v. 68, p. 390-394.

King, M. D., Closs, J., Spangler, S. and Greenstone, R. (2003): EOS Data Products Handbook NASA Goddard Space Flight Center Greenbelt, Maryland vol. 1. p57

Fujisada H, Sakuma F, Ono A, Kudoh M. (1995): Design and preflight performance of ASTER instrument protoflight model IEEE Transactions on Geoscience and Remote Sensing 1998; 36: 1152-1160

Horig, B., Kuhn, F. and Lehman, F. (2001): HyMap Hysperspectral Remote Sensing to Detect Hydrocarbons. International Journal of Remote Sensing, 2001 (22) 8; p 1413-1422.

Hughes, L. J., K. L. Zonge, and N. R. Carlson. (1986): The application of electrical techniques in mapping hydrocarbon-related alteration, *in* M. J. Davidson, ed., Unconventional methods in exploration for petroleum and natural gas, symposium IV: Dallas, Texas, Southern Methodist University Press, p. 5–26.

Hunt, J. M. (1979): *Petroleum Geochemistry and Geology*, W. H., Freeman Co. Wilson, R. D., Monaghan P. H., Osanik, A., Price, L. C., and Rogers, M. A., 1974. "Natural Marine Oil Seepage", *Science*, v. 184, p. 857-864.

Hunt, G. R. (1977): Spectral signatures of particulate minerals in the visible and near infrared. Geophysics, 42(3), 501– 513.

Hunt, G. R., Salisbury, J. W., & Lenhoff, C. R. (1972): Visible and nearinfrared spectra of minerals and rocks: V. Halides, phosphates, arsenates, vanadates, and borates. Modern Geology, 3, 121– 132.

Kahle, A. B., Palluconi, F. D., Hook, S. J., Realmuto, V.J. and Bothwell, G. (1991): The Advanced Spaceborne Thermal Emission and Reflectance Radiometer (ASTER). International Journal of Imaging Sys. Techn. 3, p 144-156.

Kaplan, A., Lusser, C.U., Norton, I.O. (1994): Tectonic map of the world, panel 10: Tulsa, American Association of Petroleum Geologists, scale 1:10,000,000.

Klett, T.R., Ahlbrandt, T.S., Schmoker, J.W., and Dolton, J.L. (1997): Ranking of the world's oil and gas provinces by known petroleum volumes: U.S. Geological Survey Open-file Report-97-463

Knipling, E. B. (1970): Physical and physiological basis for the reflectance of visible and near-infrared radiation from vegetation. Remote Sensing of Environment, 1, 155– 159.

Kulke, H., (1995): Nigeria, *in,* Kulke, H., ed., Regional Petroleum Geology of the World. Part II: Africa, America, Australia and Antarctica: Berlin, Gebrüder Borntraeger, p. 143-172.

Kuhn, F., Oppermann, K. and Horig, B. (2004): Hydrocarbon Index – an algorithm for hyperspectral detection of hydrocarbons. Int. J. Remote Sensing, 20 June, 2004, vol. 25, No. 12, 2467-2473.

Lang, H. R. and P.H. Nadeau. (1985): Petroleum commodity report-summary of results obtained at the petroleum test sites, in M. J. Abrams, J. E. Conel, H. R. and H, N. Paley, eds, The Joint NASA/Geosat Test Case Project: final report: AAPG Special Publication, pt.2, vol.2, p.10-1-10-28.

Link, W. K. (1952): "Significance of Oil and Gas Seeps in World Oil Exploration", *AAPG Bull.*, 6(8), p. 1505-1540.

Louglin, W. (1991): Principal Component Analysis for Alteration Mapping. Photogrammetric Engineering and Remote Sensing, 57, 1163-1169.

Luyendyk, B., Washburn, L., Banerjee, S., Clark J. and Quigley D. (2003): A Methodology for Investigation of Natural Hydrocarbon Gas Seepage in the Northern Santa Barbara Channel. Coastal Marine Institute, Santa Barbara, CA.

Mathews, M.D. (1986): The effects of hydrocarbon leakage on earth surface materials, in M. J. Davidson, ed., Unconventional methods in exploration for petroleum and natural gas, symposium IV: Dallas, Texas, Southern Methodist University Press, p. 27-44

Noomen, M. F., Skimore A. K. and van der Meer, F. (2003): Detecting the influence of gas seepage on vegetation using hyperspectral remote sensing. Retrieved February 17, 2005, from ITC website: http://www.itc.nl/library/Papers_2003/peer_ref_conf/noomen.pdf.

Petroconsultants, (1996): Petroleum exploration and production database: Houston, Texas, Petroconsultants, Inc., [database available from Petroconsultants, Inc., P.O. Box 740619, Houston, TX 77274-0619]

Rowan L. (2001): Advances in Lithologic Mapping by Using Optical Remote Sensing Measurement. GSA Annual Meeting, Nov. 5-8. Paper No. 145-0.

Rowan, L. C., Kingston, M. J., & Crowley, J. K. (1986): Spectral reflectance of carbonatite and related alkalic igneous rocks from four North American localities. Economic Geology, 81, 857– 871.

Ruiz-Armenta, J. R., and Prol-Ledesma, R. M., 1998, Techniques for enhancing the spectral response of hydrothermal alteration minerals in Thematic Mapper images of Central Mexico. International Journal of Remote Sensing, 19, 1981–2000.

Saunders, D. F., Burson, K. R., Thompson, C. K. (1999): Model for hydrocarbon microseepage and near-surface alterations. AAPG Bulletin, 83, 170-185

Segal, D. B., and Merin, I. S. (1989): Successful use of Landsat Thematic Mapper data for mapping hydrocarbon microseepage-induced mineralogic alteration, Lisbon Valley, Utah. Photogrammetric Engineering and Remote Sensing, 55, 1137± 1145.

Scholte, K., Garcia-Haro, J. and Kemper, T. (2004): Variable Multiple Endmember Spectral Mixture Analysis for Geology Applications. Remote Sensing Image Analysis Including the Spatial Domain, edited by Steven M. de Jong and Freek D. van der Meer. P 180-200

Schumacher, D. (1996): Hydrocarbon-Induced alteration of Soils and Sediments, in D. Schumacher and M. A. Abrams, eds., Hydrocarbon Migration and its near Surface Expression: AAPG Memoir 66, p. 71-89

Schumacher, D. (1999): Surface Geochemical Exploration for Petroleum: Chapter 18. Retrieved November 26, 2004, from http://www.gmtgeochem.com/pdf/ch18.pdf.

Schumacher, D. and Abrams, A. A. (1996): Hydrocarbon microseepage and its near-surface expression. AAPG Memoir 66

Shippert P. (2003): Introduction to hyperspectral image analysis. Research Systems, Inc. Retrieved November 20, 2004, from http://satjournal.tcom.ohiou.edu/pdf/shippert.pdf

Singh, A., and Harrison, A. (1985): Standardized Principal Components. International Journal of remote sensing, vol. 6, no. 6, p.883-896

SOUZA FILHO, C. R., and DRURY, S. A., 1998, Evaluation of JERS-1 (FUYO-1) OPS and Landsat TM images for mapping of gneissic rocks in arid areas. International Journal of Remote Sensing, 19, 3569–3594.

Staskowski, J. R. (2004): Utility of ASTER for Detecting Hydrocarbon. Geochemical Exploration for oil and gas. Retrieved January 4, 2005, from http://aapg.confex.com/aapg/da2004/techprogram/A87631.htm

TANGESTANI, M. H., and MOORE, F., 2001, Comparison of three principal component analysis techniques to porphyry copper alteration mapping: a case study in Meiduk area, Kerman, Iran. Canadian Journal of Remote Sensing, 27, 176–182.

TANGESTANI, M. H., and MOORE, F., 2002, Porphyry copper alteration mapping at the Meiduk area, Iran. International Journal of Remote Sensing, 23, 4815–4826.

Tedesco, S. A. (1995): Surface geochemistry in petroleum exploration. New York. Chapman & Thomas, J.R. and Gausman, H. W. 1977. Leaf reflectance vs. leaf chlorophyll and carote concentrations for eight crops. Agronomy Journal, 69, 799-802

Van der Meer, F., van Dijk, P., van der Werff, H., Yang, H. (2002): Remote sensing and petroleum seepage: a review and case study. Terra Nova. Vol. 14, issue 1, p1.

van der Werff, H. and Lucieer Arko. (2004): A Contextual Algorithm for Detection of Mineral Alteration Halos with Hyperspectral Remote Sensing, Remote Sensing Image Analysis Including the Spatial Domain, edited by Steven M. de Jong and Freek D. van der Meer. P 201-210

Yamaguchi Y, Kahle A. B, Tsu H, Kawakami T, Pniel , M. (1998): Overview of Advanced Spaceborne Thermal Emission and Reflection Radiometer (ASTER) IEEE Transactions on Geoscience and Remote Sensing 1998; 36: 1062-1071

Yuhas, R.H., Goetz, A. F. H., and Boardman, J. W. (1992): Discrimination among semiarid landscape endmembers using the spectral angle mapper (SAM) algorithm. In Summaries of the Third Annual JPL Airborne Geoscience Workshop, JPL Publication 92-14, vol. 1, pp. 147-149.

APPENDICES

I: Picture showing oil-farm tanks common within the two test sites

II: Picture showing oil terminal and hydrocarbon flares common in both test sites used for the study

III: Picture showing wind speed and direction, gotten same day with test site I image (source: http://podaac.jpl.nasa.gov/quikscat/qscat_browse.html)

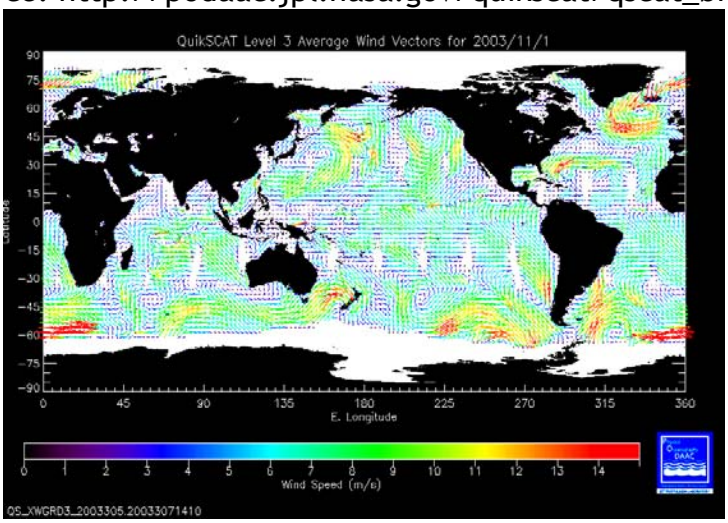

IV: Picture showing wind speed and direction, gotten same day with test site II image (source: http://podaac.jpl.nasa.gov/quikscat/qscat_browse.html)

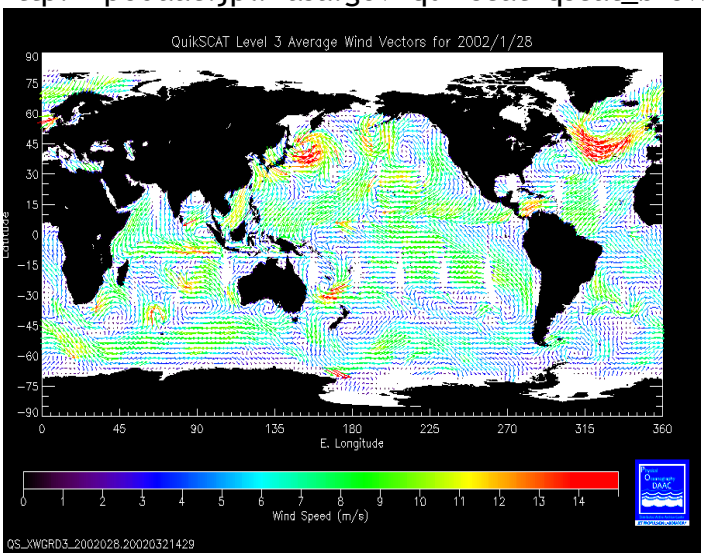

V: Hydrocarbon Flares and Flare like pixels mapping the pattern of the flare extent in test site I